Title: Maturing Mycobacterial Peptidoglycan Requires Non-canonical Crosslinks to Maintain Shape

Authors: Catherine Baranowski[1], Michael A. Welsh[2], Lok-To Sham[2,3], Haig A. Eskandarian[4,5], Hoong C. Lim[2], Karen J. Kieser[1], Jeffrey C. Wagner[1], John D. McKinney[4], Georg E. Fantner[5], Thomas R. Ioerger[6], Suzanne Walker[2], Thomas G. Bernhardt[2], Eric J. Rubin[1,2]*, E. Hesper Rego[7*]

Affiliations:

[1] Department of Immunology and Infectious Disease, Harvard T. H. Chan School of Public Health, Boston, MA 02115, USA; [2] Department of Microbiology and Immunobiology, Harvard Medical School, Boston, MA 02115, USA; [3] Department of Microbiology and Immunology, National University of Singapore, 117545 Singapore; [4] School of Life Sciences, Swiss Federal Institute of Technology in Lausanne (EPFL), 1015 Lausanne, Switzerland; [5] School of Engineering, Swiss Federal Institute of Technology in Lausanne (EPFL), 1015 Lausanne, Switzerland; [6] Department of Computer Science and Engineering, Texas A&M University, College Station, Texas, USA;[7] Department of Microbial Pathogenesis, Yale University School of Medicine, New Haven, Connecticut, 06510, USA.

* to whom correspondence should be addressed: erubin@hsph.harvard.edu; hesper.rego@yale.edu

Abstract:

In most well studied rod-shaped bacteria, peptidoglycan is primarily crosslinked by penicillin binding proteins (PBPs). However, in mycobacteria, L,D-transpeptidase (LDT)-mediated crosslinks are highly abundant. To elucidate the role of these unusual crosslinks, we characterized mycobacterial cells lacking all LDTs. We find that LDT-mediated crosslinks are required for rod shape maintenance specifically at sites of aging cell wall, a byproduct of polar elongation. Asymmetric polar growth leads to a non-uniform distribution of these two types of crosslinks in a single cell. Consequently, in the absence of LDT-mediated crosslinks, PBP-catalyzed crosslinks become more important. Because of this, *Mycobacterium tuberculosis* (Mtb) is more rapidly killed using a combination of drugs capable of PBP- and LDT- inhibition. Thus, knowledge about the single-cell distribution of drug targets can be exploited to more effectively treat this pathogen.

Introduction:

Peptidoglycan (PG) is an essential component of all bacterial cells (Vollmer, Blanot, & de Pedro, 2008a), and the target of many antibiotics. PG consists of linear glycan strands crosslinked by short peptides to form a continuous molecular cage surrounding the plasma membrane. This structure maintains cell shape and protects the plasma membrane from rupture. Our understanding of PG is largely derived from studies on laterally growing model rod-shaped bacteria like *Escherichia coli* and *Bacillus subtilis* (*Figure 1 - figure supplement 1A*). In these organisms, new PG is constructed along the

45 lateral side wall by the concerted effort of glycoslytransferases, which connect the glycan
46 of a new PG subunit to the existing mesh, and transpeptidases, which link peptide side
47 chains. An actin-like protein, MreB, positions this multi-protein complex along the short
48 axis of the cell so that glycan strands are inserted circumferentially, creating
49 discontinuous hoops of PG around the cell (Domínguez-Escobar et al., 2011; Garner et
50 al., 2011). This orientation of PG creates a mechanical anisotropy that is responsible for
51 rod shape (Hussain et al., 2018).

52 However, not all rod-shaped bacteria encode MreB. In fact, there are important
53 differences between model bacteria and Actinobacteria like mycobacteria, a genus of rod-
54 shaped bacteria that includes the major human pathogen *Mycobacterium tuberculosis*
55 (Mtb). In mycobacteria, new PG is inserted at the cell poles (at unequal amounts based
56 on pole age), rather than along the lateral walls (*Figure 1A*). Additionally, mycobacteria
57 are missing several factors, including MreB, that are important for cell elongation (Kieser
58 & Rubin, 2014). Furthermore, in *E. coli* and *B. subtilis* the vast majority (>90%) of the
59 peptide linkages are created by D,D-transpeptidases known as penicillin binding proteins
60 (PBPs) (Pisabarro, de Pedro, & Vázquez, 1985). PBPs, the targets of most β-lactams,
61 link the 4th amino acid of one peptide side chain to the 3rd amino acid of another, forming
62 4-3 crosslinks (*Figure 1- figure supplement 1B*). Peptide linkages can also be catalyzed
63 by L,D-transpeptidases (LDTs), which link peptide side chains by the 3rd amino acid
64 forming 3-3 linkages. In mycobacteria, these 3-3 crosslinks, are highly abundant,
65 accounting for ~60% of linkages (Kumar et al., 2012) (*Figure 1- figure supplement 1B*).
66 Because PG has been most well studied in bacteria where 3-3 crosslinks are rare, the

67 role of these linkages, and the enzymes that catalyze their formation, is poorly
68 understood.

69 Tuberculosis remains an enormous global health problem, in part, because
70 treating even drug susceptible disease is difficult. The standard regimen includes a
71 cocktail of four drugs given over six months. Treatment of drug-resistant Mtb is
72 substantially longer and includes combinations of up to seven drugs ("Global Tuberculosis
73 Report 2017," 2017). While some of the most important anti-mycobacterials target cell
74 wall synthesis, surprisingly, drugs that target PG are not part of the core treatment for
75 either drug-susceptible or drug-resistant disease. However, carbapenems, β-lactam
76 antibiotics that potently inhibit LDTs *in vitro*, are effective against drug resistant Mtb *in*
77 *vitro* and drug sensitive Mtb in patients (Diacon et al., 2016; Hugonnet, Tremblay, Boshoff,
78 Barry, & Blanchard, 2009).

79 But, why are LDTs important in mycobacteria? To explore this, we constructed
80 strains that lack the ability to form 3-3 crosslinks. We find that 3-3 crosslinks are formed
81 in maturing peptidoglycan and that they are necessary to stabilize the cell wall and
82 prevent lysis. Cells that lose the ability to synthesize 3-3 crosslinks have increased
83 dependence on 4-3 crosslinking. Thus, simultaneous inhibition of both processes results
84 in rapid cell death.

85

86 **Results:**

87 **Fluorescent D-amino acids are incorporated asymmetrically by LD-**
88 **transpeptidases**

89 PG uniquely contains D-amino acids, which can be labeled with fluorescent probes
90 (fluorescent D-amino acids, FDAAs) to visualize PG synthesis in live bacterial cells (Kuru
91 et al., 2012). When we incubated *M. smegmatis* (Msm), a non-pathogenic relative of Mtb,
92 with FDAAs for a short 2-minute pulse (< 2% of Msm's generation time) we observed
93 incorporation at both poles, the sites of new PG insertion in mycobacteria (*Figure 1A, B*)
94 (Aldridge et al., 2012). However, we also saw a gradient of fluorescence along the
95 sidewalls, extending from the old pole (the previously established growth pole) that fades
96 to a minimum at roughly mid-cell as it reaches the new pole (the pole formed at the last
97 cell division) (*Figure 1B*).

98 To identify the enzymes responsible for this unexpected pattern of lateral cell wall
99 FDAA incorporation, we performed a fluorescence-activated cell sorting (FACS)-based
100 transposon screen (*Figure 1C*). Briefly, we stained an Msm transposon library with FDAA
101 and repeatedly sorted the least fluorescent 12.5% of the population by FACS. After each
102 sort we regrew cells, extracted gDNA and used deep sequencing to map the location of
103 the transposons found in the low staining population.

104 From this screen, we identified three LDTs (*ldtA - MSMEG_3528, ldtB -*
105 *MSMEG_4745, ldtE - MSMEG_0233*) (*Figure 1D*) that were primarily responsible for
106 FDAA incorporation. Deleting these three LDTs significantly reduced FDAA incorporation
107 (*Figure 1- figure supplement 2A, B*). To further investigate the physiological role of LDTs,
108 we constructed a strain lacking all 6 LDTs (Δ*ldtAEBCGF*, hereafter ΔLDT). FDAA
109 incorporation and 3-3 crosslinking are both nearly abolished in ΔLDT cells and can be
110 partially restored by complementation with a single LDT (*ldtE*-mRFP; ΔLDT_{comp}) (*Figure*
111 *1E, F, Figure 1- figure supplement 2C, 3*). Thus, as might be the case in *Bdellovibrio*

112 (Kuru et al., 2017), FDAA incorporation in Msm is primarily LDT-dependent. LDTs have
113 previously been shown to exchange non-canonical D-amino acids onto PG tetrapeptides
114 in *Vibrio cholera* (Cava, de Pedro, Lam, Davis, & Waldor, 2011).
115

116 **LDT catalyzed 3-3 crosslinks are required for rod shape maintenance at aging cell**
117 **wall**

118 As deletion of a subset of LDTs in Msm produces morphologic changes (Sanders,
119 Wright, & Pavelka, 2014), we visualized ΔLDT cells by time-lapse microscopy. We
120 observed that a subpopulation of cells loses rod shape progressively over time, resulting
121 in localized spherical blebs (*Figure 2A - top, Figure 2 - figure supplement 1A, Figure 2 -*
122 *video 1*). Complemented cells are able to maintain rod shape (*Figure 2 - figure*
123 *supplement 1B*). We reasoned that localized loss of rod shape may occur for two reasons:
124 1) spatially-specific loss of cell wall integrity and/or 2) cell wall deformation due to
125 uncontrolled, local PG synthesis. If the first hypothesis were true, high osmolarity should
126 protect cells against forming blebs. Indeed, switching cells from iso- to high- osmolarity
127 prevented bleb formation over time (*Figure 2A, bottom, Figure 2- video 2*). To test the
128 second hypothesis, we stained ΔLDT cells with an amine-reactive dye, and observed
129 outgrowth of new, unstained material (*Figure 2B*). Blebs retained stain, indicating a lack
130 of new cell wall synthesis in the region. Collectively, these results indicate that 3-3
131 crosslinks are required to counteract turgor pressure and maintain the rod shape of
132 mycobacteria. This led us to hypothesize that bleb formation is a result of a local defect
133 in cell wall rigidity.

134 To directly measure cell wall rigidity, we used atomic force microscopy (AFM) on
135 live ΔLDT and WT cells. We measured the rigidity of cells in relation to their height.
136 Generally, WT cells are stiffer than ΔLDT cells (*Figure 2D*). Blebs in ΔLDT cells can be
137 identified by a sharp increase in height (*Figure 2E, pink shaded*). Since circumferential
138 stress of the rod measured by AFM is proportional to the radius of the cell, and inversely
139 proportional to the thickness of the cell wall (an immeasurable quantity by AFM), we used
140 cell height, a proxy for radius, to normalize the stiffness measurement. We found that
141 stiffness drops in the area of blebs (*Figure 2E, pink shaded*).

142 Why does loss of rod shape occur locally and only in a subpopulation of cells?
143 Mycobacterial polar growth and division results in daughter cells with phenotypic
144 differences (Aldridge et al., 2012). For example, the oldest cell wall is specifically inherited
145 by the new pole daughter (*Figure 2- supplement 2A*, (Aldridge et al., 2012)). We
146 hypothesized that the loss of rod shape might occur in specific progeny generated by cell
147 division. Indeed, the daughter which inherited the new pole from the previous round of
148 division, and the oldest cell wall, consistently lost rod shape over time, while the old pole
149 daughter maintained rod shape (*Figure 2C, Figure 2- supplement 2B*). In addition, blebs
150 localized to the oldest cell wall (*Figure 2B*), as visualized by pulse-chase labeling of the
151 cell wall. Thus, 3-3 crosslinking is likely occurring in the oldest cell wall, which is non-
152 uniformly distributed along a single cell and in the population via asymmetric polar growth
153 and division. Taken together, these data suggest that LDTs act locally to reinforce aging
154 PG and to maintain rod shape in a subpopulation of Msm cells - specifically, new pole
155 daughters (*Figure 2F*).

156

157 **Mycobacteria are hypersensitive to PBP inactivation in the absence of LDTs**

158 Our observations lead to the following model (*Figure 6A*): PBP-catalyzed 4-3
159 crosslinks are formed at the poles where new PG is inserted and where pentapeptide
160 substrates reside. These newly synthesized 4-3 crosslinks are then gradually cleaved (by
161 D,D-endopeptidases) as PG ages and moves toward the middle of the cell, leaving
162 tetrapeptide substrates for LDTs to create 3-3 crosslinks. This is consistent with the FDAA
163 incorporation pattern, which reflects the abundance of tetrapeptide substrates available
164 for LDT exchange. Specifically, there are more available tetrapeptides near the poles and
165 fewer near mid-cell, the site of older PG (*Figure 1F*). In the absence of LDTs to catalyze
166 3-3 crosslinks, old cell wall loses integrity and turgor pressure causes bleb formation.

167 This model predicts that ΔLDT cells should be even more dependent on 4-3
168 crosslinking than wild type cells. To test this hypothesis, we used TnSeq (Long et al.,
169 2015) to identify genes required for growth in cells lacking LDTs (*Figure 3A*). We found
170 that mutants of two PBPs, *pbpA (MSMEG_0031c)* and *ponA2 (MSMEG_6201)*, were
171 recovered at significantly lower frequencies in ΔLDT cells (*Figure 3B*). Likewise, using
172 allele swapping (Kieser, Boutte, et al., 2015b) (*Figure 3C, Figure 3- figure supplement*
173 *1A*), a technique that tests the ability of various alleles to support viability, we found that
174 the transpeptidase (TP) activity of PonA1, which is non-essential in WT cells (Kieser,
175 Boutte, et al., 2015b), becomes essential in ΔLDT cells (*Figure 3D*). Thus, cells that lack
176 3-3 crosslinks are more dependent on 4-3 crosslinking enzymes.

177

178 **Peptidoglycan synthesizing enzymes localize to differentially aged cell wall**

179 Given our model, we hypothesized that enzymes catalyzing and processing
180 different types of crosslinks should be differentially localized along the length of the cell.
181 Specifically, we postulated that 4-3 crosslinking PBPs would localize at sites of new PG,
182 while 4-3 cleaving D,D-endopeptidases and 3-3 crosslinking LDTs would localize to sites
183 of older PG. To test whether 3-3 and 4-3 crosslinking enzymes localize differently, we
184 visualized fluorescent fusions of a PBP (PonA1), and an LDT (LdtE), (*Figure 4A*). We
185 found that PonA1-RFP largely localized to the old pole, where new PG is inserted (*Figure*
186 *4A, B, Figure 4 - video 1*). LdtE-mRFP localized farther from the poles, the sites of older
187 PG (*Figure 4A, B, Figure 4 - video 2*). Thus, enzymes responsible for 4-3 and 3-3
188 crosslinks exhibit distinctive subcellular localizations, consistent with the model that they
189 act on differentially aged PG.

190 We next sought to localize a D,D-endopeptidase. As no D,D-endopeptidase has
191 been clearly identified in mycobacteria, we used HHPRED (Zimmermann et al., 2017) to
192 find candidates. By homology to the *E. coli* protein AmpH, an enzyme with both D,D-
193 carboxy- and endopeptidase activity (González-Leiza, de Pedro, & Ayala, 2011), we
194 identified DacB2 (MSMEG_2433), a protein previously shown to have D,D-
195 carboxypeptidase activity in Msm (Bansal et al., 2015), as a candidate to also harbor D,D-
196 endopeptidase capability. We expressed and purified DacB2 and found that it, like AmpH,
197 had both D,D-carboxypeptidase and D,D-endopeptidase activity on peptidoglycan
198 substrates generated *in vitro* (*Figure 4C, Figure 4- figure supplement 1A-C*). Consistent
199 with our model, DacB2-mRFP localized closer to LDT-mRFP, farther from the poles, at
200 sites of older PG (*Figure 4A, B, Figure 4 – video 3*). Thus, bleb formation may result from
201 unchecked D,D-endopeptidase activity in ΔLDT cells.

202 **Drugs targeting both PBPs and LDTs synergize to kill Mtb**

203 The importance of 3-3 crosslinks in mycobacteria suggests a unique vulnerability.
204 While Mtb can be killed by most non-carbapenem (N-C) β-lactams like penicillins, which
205 largely target the PBPs, carbapenem β-lactams, which target both PBPs and LDTs
206 (Mainardi et al., 2007; Papp-Wallace, Endimiani, Taracila, & Bonomo, 2011) are also
207 effective against Mtb (Diacon et al., 2016; Hugonnet et al., 2009). As has been previously
208 proposed (Gonzalo & Drobniewski, 2013; Gupta et al., 2010; Mainardi et al., 2007), our
209 data suggest that more rapid killing of Mtb could be achieved with drug combinations that
210 target both PBPs and LDTs (*Figure 5A*). In fact, we find that the combination of amoxicillin
211 (a penicillin) and meropenem (a carbapenem), exhibits synergism in minimal inhibitory
212 concentration (Σ Fractional Inhibitory Concentration < 0.5 ("Synergism Testing: Broth
213 Microdilution Checkerboard and Broth Macrodilution Methods," 2016), *Figure 5B, Figure*
214 *5- figure supplement 1A,B*). We also see that this combination leads to more rapid killing
215 of Mtb *in vitro* (*Figure 5B, Figure 5- figure supplement 2A*) (Andreu, Fletcher, Krishnan,
216 Wiles, & Robertson, 2012).

217

218 **Discussion:**

219 The success of antibiotics that target PG, like β-lactams, has led to decades of
220 research of this critical bacterial polymer. Recently developed fluorescent probes
221 (FDAAs) of PG synthesis have been used extensively to study PG-synthesis in live cells
222 of numerous bacterial species. Intriguingly, these probes can be incorporated through
223 diverse pathways in different bacteria and thus, their pattern can mark distinct processes
224 (Kuru et al., 2012). Here, we find that, in mycobacteria, FDAA incorporation is primarily

225 LDT-dependent. FDAA incorporation in Msm shows an unusual gradient pattern (Botella
226 et al., 2017), suggesting an asymmetric distribution of tetrapeptide substrate for the LDT-
227 dependent exchange reaction. In addition to their ability to exchange D-amino acids onto
228 tetrapeptides, LDTs also catalyze non-canonical 3-3 crosslinks.

229 LDT-catalyzed crosslinks are rare in model rod-shaped bacteria like *E.coli* and *B.*
230 *subtilis* but, are abundant in polar growing bacteria like mycobacteria, *Agrobacterium*
231 *tumefaciens* and *Sinorhizobium meliloti* (Brown et al., 2012; Cameron, Zupan, &
232 Zambryski, 2015; Kumar et al., 2012; Lavollay et al., 2008; Pisabarro et al., 1985). Here,
233 we find that Msm cells lacking 3-3 crosslinks cannot maintain rod shape at sites of aging
234 cell wall. PBP-catalyzed 4-3 crosslinks appear able to maintain rod shape near the poles,
235 the sites of newer cell wall (*Figure 6A*). Over time, older cell wall moves towards the
236 middle of the cell, loses structural stability, and begins to bleb. The gradual manner in
237 which rod shape is lost suggests that cell wall processing must occur to de-stabilize this
238 portion of the rod. Consistent with this idea, we find that an enzyme that cleaves 4-3
239 crosslinks, DacB2, also localizes to sites of old cell wall.

240 Why would Msm cells create 4-3 crosslinks to eventually cleave them? There are
241 many possibilities. For example, perhaps in the absence of lateral cell wall synthesis, the
242 creation of substrate for LDTs through the destruction of 4-3 crosslinks allows the cell to
243 engage the PG along the lateral cell body. This could be important for altering the
244 thickness of the PG layer or anchoring it to the membrane at sites of otherwise “inert” cell
245 wall. Additionally, it may be that as PG ages, it is being manicured for septal synthesis.
246 Supporting this idea, we find that the localization patterns of PonA1, LdtE and DacB2,
247 and FDAA all have local minima at mid-cell closer to the new pole, the asymmetric site of

248 division in mycobacteria (Aldridge et al., 2012; Dhar, Bousbaine, Wakamoto, McKinney,
249 & Santi, 2013; Eskandarian et al., 2017). This lack of localization suggests a lack of penta-
250 and tetra- peptide substrates, implying that that this region of the cell more abundantly
251 crosslinked, as crosslinking utilizes these peptide species. Mycobacteria are missing
252 known molecular septal placement mechanisms like the Noc and the Min system (Hett &
253 Rubin, 2008). Could 3-3 crosslinking be a signal for septal placement? Indeed, the major
254 septal PG hydrolase is RipA, a D,L-endopeptidase which cleaves the bond between the
255 second and third amino acid of PG side chains, a substrate available on 3-3 crosslinked
256 material (Böth, Schneider, & Schnell, 2011; Vollmer, Joris, Charlier, & Foster, 2008b).
257 Thus, it is intriguing to speculate that 3-3 crosslinks could be important for localizing cell
258 division machinery.

259 In well-studied rod-shaped bacteria like *E.coli* and *B. subtilis*, shape is maintained
260 by MreB-directed PG synthesis along the lateral cell body (Garner et al., 2011; Hussain
261 et al., 2018; Ursell et al., 2014). On the other hand, mycobacteria maintain shape in the
262 absence of an obvious MreB homolog, and in the absence of lateral cell wall elongation.
263 Furthermore, in contrast to lateral-elongating bacteria, in which new and old cell wall are
264 constantly intermingled during growth, polar growth segregates new and old cell wall
265 (*Figure 6B*). We find that mycobacteria appear to utilize 3-3 crosslinks at asymmetrically
266 distributed aging cell wall to provide stability along the lateral body, something that may
267 not be required in the presence of MreB-directed PG synthesis.

268 New drug combinations for TB are desperately needed. Indeed, there has been a
269 renewed interest in repurposing FDA-approved drugs for TB treatment (Diacon et al.,
270 2016). Our results suggest that a better understanding of the localization and distribution

271 of drug targets in single cells may lead to rational predictions of drug combinations.
272 Indeed, we find that enzymes which do very similar chemistry – PG crosslinking – are
273 distributed differentially in a single cell and across the population. In the absence of 3-3
274 crosslinks, 4-3 crosslinks become more important for cell viability. These data predict that
275 a drug combination which inhibits both PBPs and LDTs will work synergistically to more
276 quickly kill Mtb, a prediction we verified *in vitro*. Interestingly, meropenem combined with
277 amoxicillin/clavulanate resulted in early clearance of Mtb from patient sputum (Diacon et
278 al., 2016). In fact, the combination might be key to accelerated killing of Mtb (Gonzalo &
279 Drobniewski, 2013).
280

281 **Acknowledgments:**

282 We thank Cara Boutte and Erkin Kuru for discussion and thorough manuscript review.
283 We are grateful to the Rubin and Fortune laboratory for discussion and input. We also
284 thank the Microbiology and Immunobiology department at Harvard Medical School for
285 sharing equipment and reagents, as well as the BSL3 staff at the Harvard School of Public
286 health for tremendous support. This work was supported by the National Institutes of
287 Health U19 AI107774 to E.J.R and T.R.I., F32AI104287 to E.H.R (who is also supported
288 by a Career Award at the Scientific Interface from BWF), R01 GM76710 to S.W.,
289 R01AI083365 and U19AI109764 to T.G.B.. M.A.W. is supported by an F32 GM123579.
290 LT.S. was supported by an American Heart Association Postdoctoral fellowship
291 (14POST18480014). H.C.L is funded by a Simons Foundation Fellow of the Life Sciences
292 Research Foundation award. This work was also supported in part by the Swiss National
293 Science Foundation (310030_156945) and the Innovative Medicines Initiative (115337)

294 to J.D.M., and from the Swiss National Science Foundation (205321_134786 and
295 205320_152675), the European Union FP7/2007-2013/ERC Grant Agreement No.
296 307338 (NaMic), and EU-FP7/Eurostars E!8213 to G.E.F. Support for H.A.E. comes from
297 a European Molecular Biology Organization Long Term Fellowships (191-2014 and 750-
298 2016). K.J.K. was supported by the National Science Foundation Graduate Research
299 Fellowship (DGE1144152, DGE0946799).
300

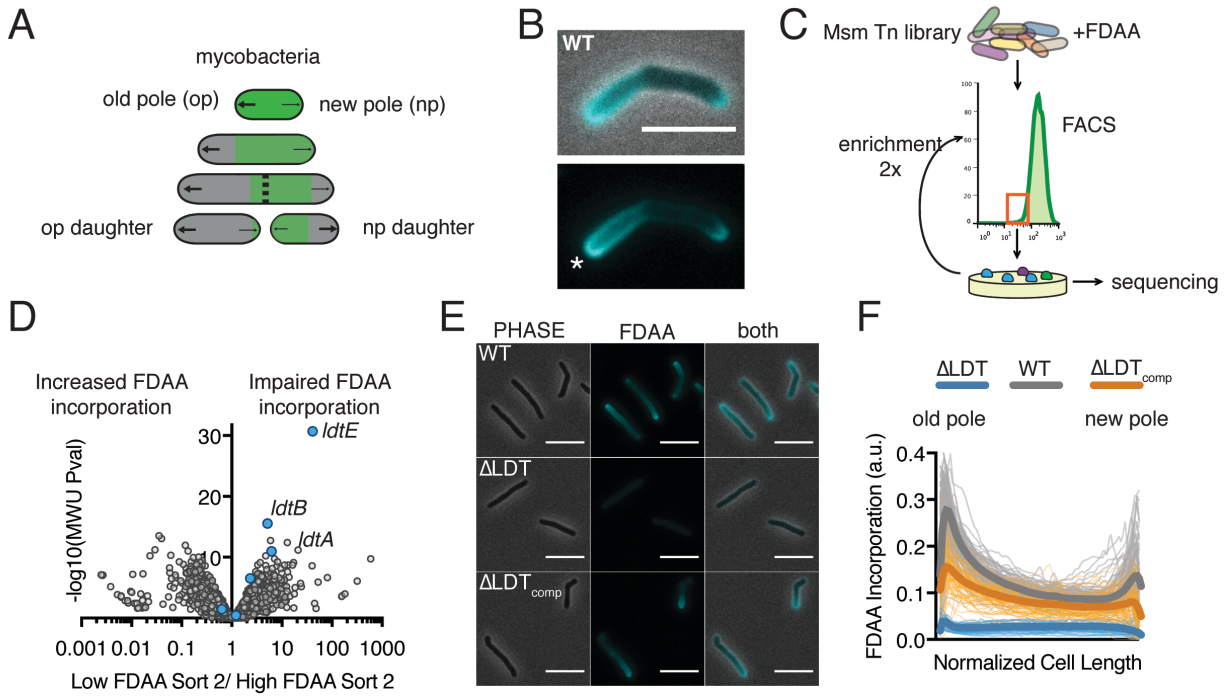

Figure 1: FDAAs are incorporated asymmetrically by LD-transpeptidases. (A) Schematic of mycobacterial asymmetric polar growth. Green, old cell wall; grey, new material; dotted line, septum; large arrows, old pole growth; small arrows, new pole growth. **(B)** FDAA incorporation in log-phase WT Msm cell after 2-minute incubation. Scale bar=5µm. Old pole marked with (*). **(C)** Schematic of Fluorescence Activated Cell Sorting (FACS)-based FDAA transposon library enrichment. An Msm transposon (Tn) library was stained with FDAAs, the dimmest and brightest cells were sorted, grown, sorted again to enrich for transposon mutants that are unable or enhanced for FDAA incorporation. **(D)** Results from 1C screen. For each gene, the contribution to low or high staining population was calculated from transposon reads per gene. Plotted is the ratio of the population contribution from the second sort of low FDAA staining (L2) over the second sort of high FDAA staining (H2) cells compared to the Mann-Whitney *U* P-value. **(E)** Representative image of FDAA incorporation in log-phase WT, ΔLDT and ΔLDT_{comp} cells. Scale bar= 5µm. **(F)** Profiles of FDAA incorporation in log-phase WT (N=98), ΔLDT (N=40), and ΔLDT_{comp} (N=77) cells. Thick lines represent mean incorporation profile, thin lines are FDAA incorporation in single cells.

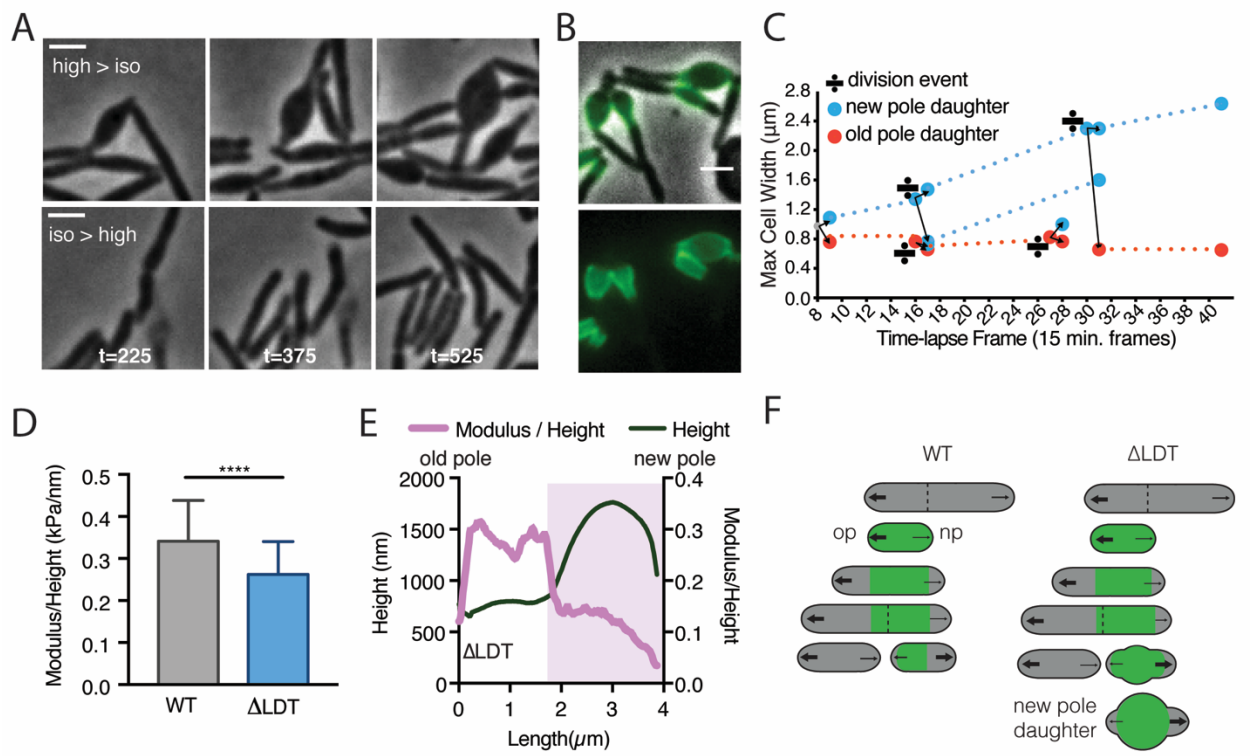

Figure 2: LDT catalyzed 3-3 crosslinks are required for rod shape maintenance at aging cell wall. (A) Msm ΔLDT time-lapse microscopy of cells switched from high- to iso- (top) osmolar media, or iso- to high osmolar media (bottom). (high=7H9+150mM sorbitol; iso=7H9). t= time in minutes post osmolarity switch. **(B)** ΔLDT cells were stained with Alexa 488 NHS-ester (green) to mark existing cell wall, washed, and visualized after outgrowth (unstained material). A, B scale bar=2µm. **(C)** Maximum cell width of ΔLDT cell lineages over time. Width of new pole daughters = blue circle; width of old pole daughters = orange circle. Division signs denote a division event. At each division, there are two arrows from the dividing cell leading to the resulting new and old pole daughter cell widths (blue and orange respectively). **(D)** Mean stiffness of WT (N=73) and ΔLDT (N=47) Msm cells as measured by atomic force microscopy. Mann-Whitney U P-Value **** < 0.0001. **(E)** Representative profile of cell height and height-normalized stiffness (modulus/height) in a single ΔLDT cell. Pink shaded portion highlights location of a bleb. **(F)** Model of rod shape loss in old cell wall of ΔLDT cells compared to WT. Green portions of the cell represents old cell wall; grey portion represents new cell wall. The larger arrows indicate more growth from the old pole, while smaller arrows show less relative growth from the new pole. Dotted lines represent septa. op= old pole, np=new pole.

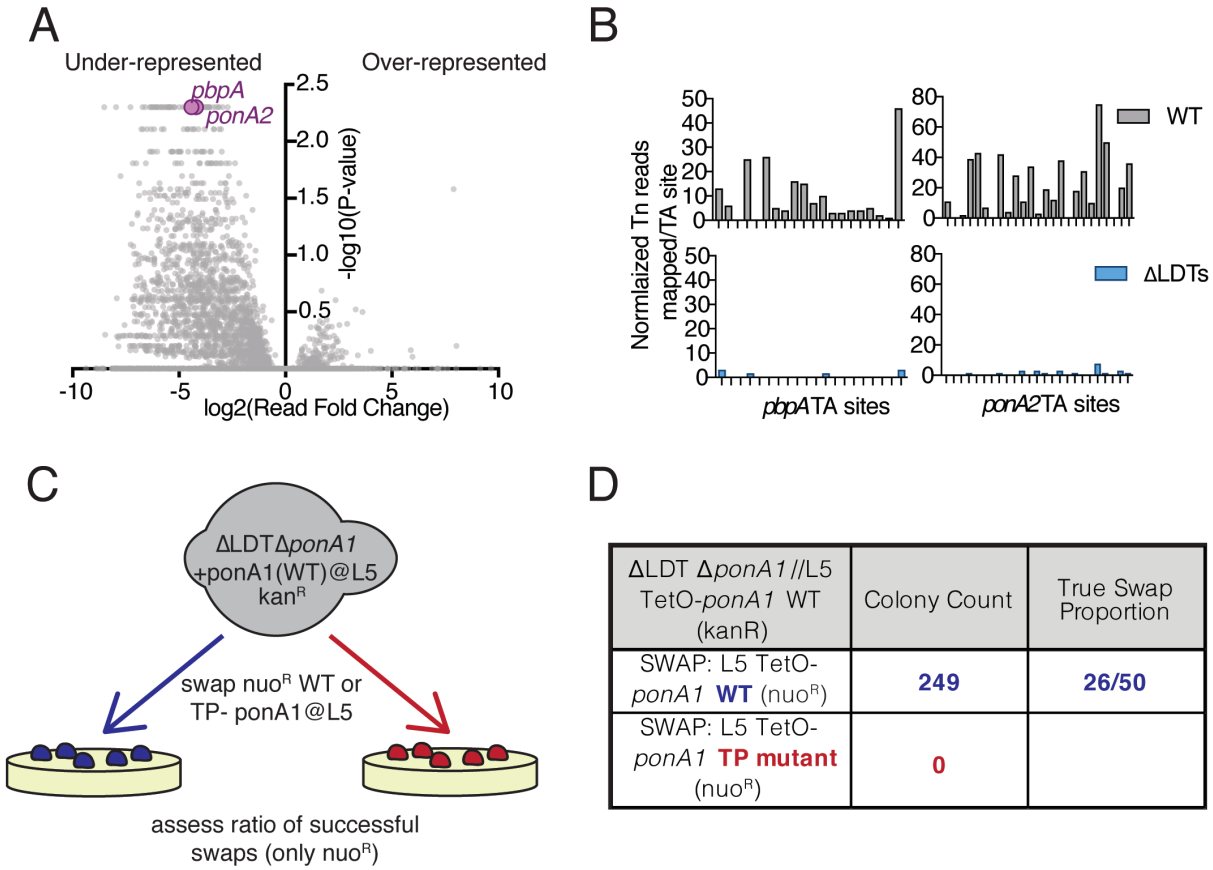

ΔLDT Δ*ponA1*//L5 TetO-*ponA1* WT (kanR)	Colony Count	True Swap Proportion
SWAP: L5 TetO-*ponA1* **WT** (nuo^R)	**249**	**26/50**
SWAP: L5 TetO-*ponA1* **TP mutant** (nuo^R)	**0**	

Figure 3: Mycobacteria are hypersensitive to PBP inactivation in the absence of LDTs. (A) Fold change in the number of reads for transposon insertion counts in ΔLDT cells compared to WT Msm. P-value is derived from a rank sum test (DeJesus, Ambadipudi, Baker, Sassetti, & Ioerger, 2015). **(B)** Transposon insertions per TA dinucleotide in *pbpA* and *ponA2* in WT (grey) and ΔLDT (blue) cells. **(C)** Schematic of L5 allele swapping experiment. Adapted from (Kieser, Boutte, et al., 2015b). **(D)** Results of WT or transpeptidase null *ponA1* allele swapping experiment in ΔLDT cells.

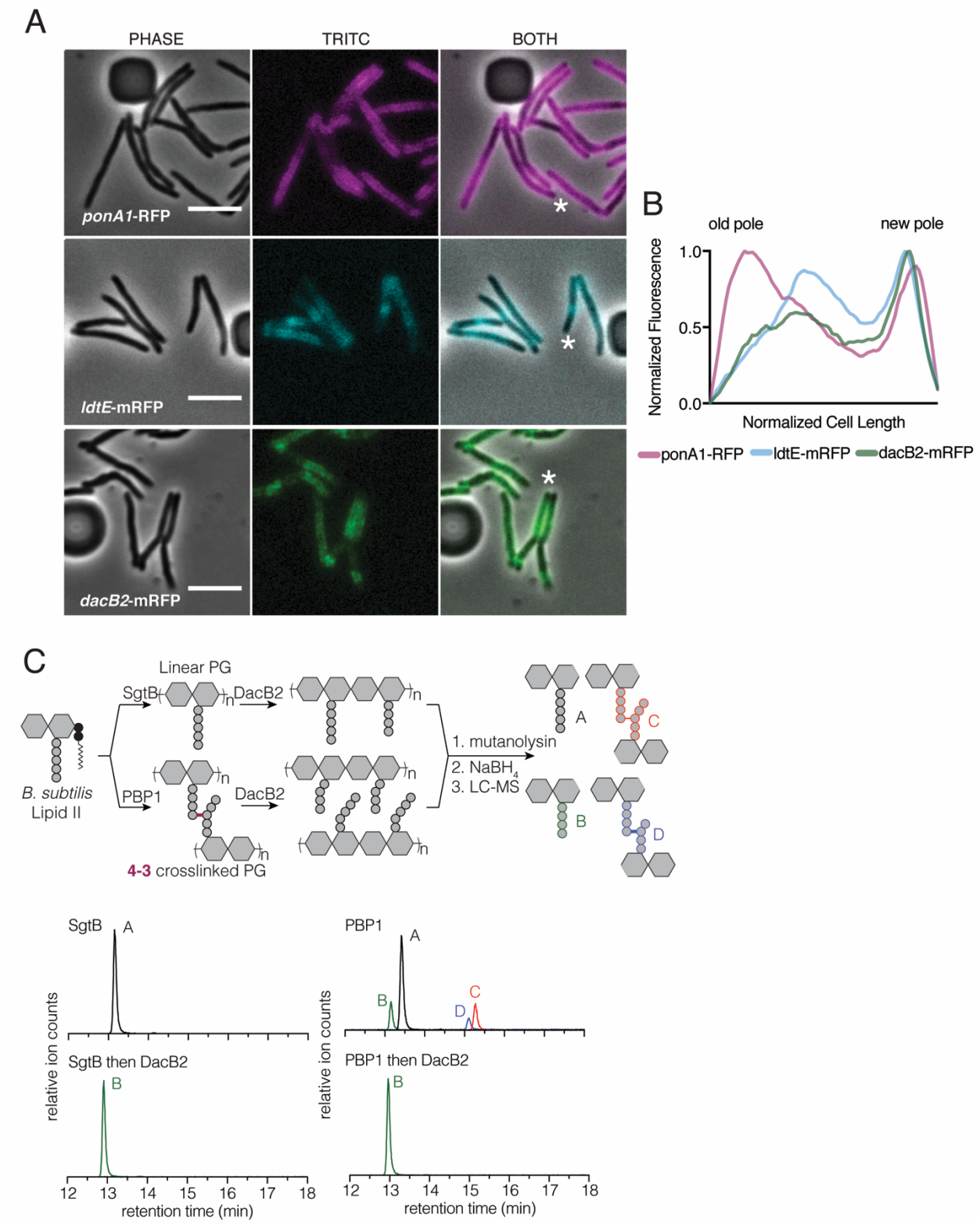

Figure 4: Peptidoglycan synthesizing enzymes localize to differentially aged cell wall. (A) Representative fluorescence images of PonA1-RFP (magenta), LdtE-mRFP (cyan), and DacB2-mRFP (green). Scale bars=5μm. **(B)** Average PonA1-RFP (N=24),

358 LdtE-mRFP (N=23) or DacB2-mRFP (N=23) distribution in cells before division. **(C)**
359 Schematic of the *in vitro* experiment to test D,D-carboxy- and D,D-endopeptidase activity
360 of DacB2. Lipid II extracted from *B. subtilis* is first polymerized into linear (using SgtB) or
361 crosslinked (using *B. subtilis* PBP1) peptidoglycan and then reacted with DacB2. The
362 reaction products are analyzed by LC-MS. **(below)** Extracted ion chromatograms of the
363 reaction products produced by incubation of DacB2 with peptidoglycan substrates.
364
365
366

367

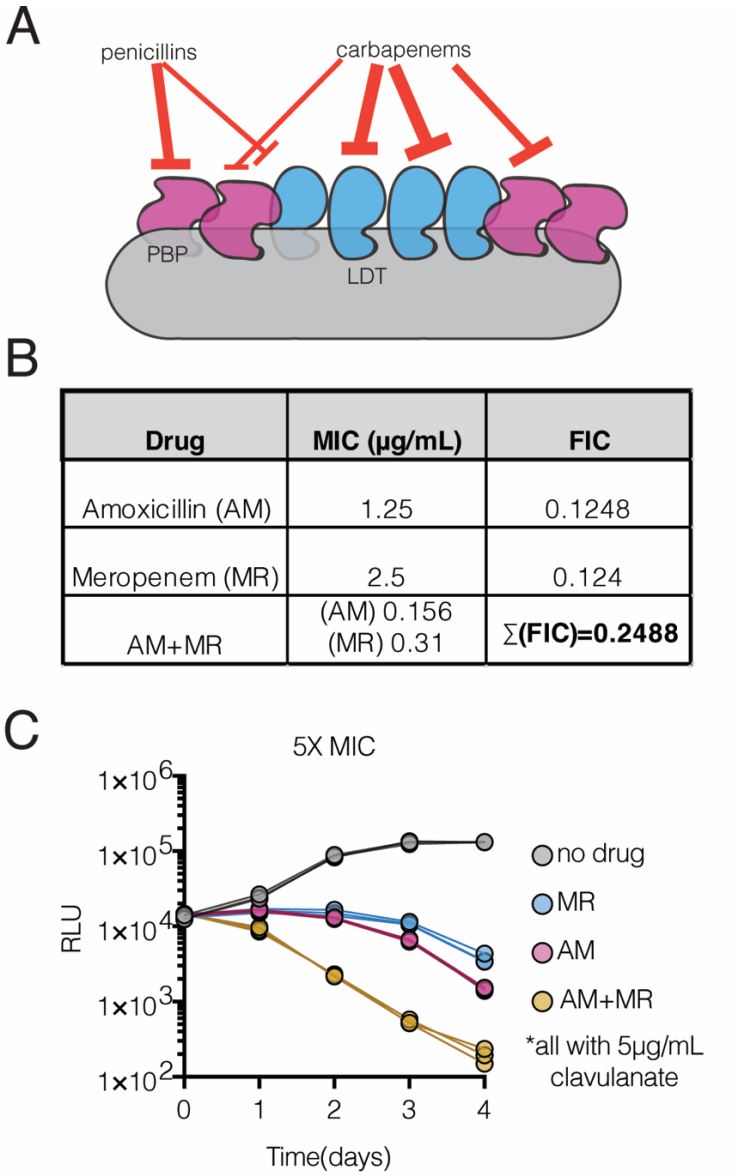

Drug	MIC (μg/mL)	FIC
Amoxicillin (AM)	1.25	0.1248
Meropenem (MR)	2.5	0.124
AM+MR	(AM) 0.156 (MR) 0.31	**∑(FIC)=0.2488**

Figure 5: Drugs targeting both PBPs and LDTs synergize to kill Mtb. (A) Schematic of synergistic targeting of PBPs and LDTs by pencillin and carbapenem β-lactams. **(B)** Minimum inhibitory concentration (MIC) of amoxicillin, meropenem, or the combination, in *M. tuberculosis*. FIC (fractional inhibitory concentration) = MIC of drug in combination/MIC of drug alone. Synergy is defined as ∑ FIC<=0.5 ("Synergism Testing: Broth Microdilution Checkerboard and Broth Macrodilution Methods," 2016). **(C)** Killing dynamics of *M. tuberculosis* (expressing the *luxABCDE* operon from *Photorhabdus luminescens* (Andreu et al., 2010)) measured via luciferase production (RLU=relative light units). 5X MIC Amoxicillin (AM) (3.125 μg/mL); 5X MIC Meropenem (MR) (6.25 μg/mL); Amoxicillin+Meropenem 3.125 μg/mL AM; 6.25 μg/mL MR). Biological triplicate are plotted. All drugs were used in combination with 5μg/mL clavulanate.

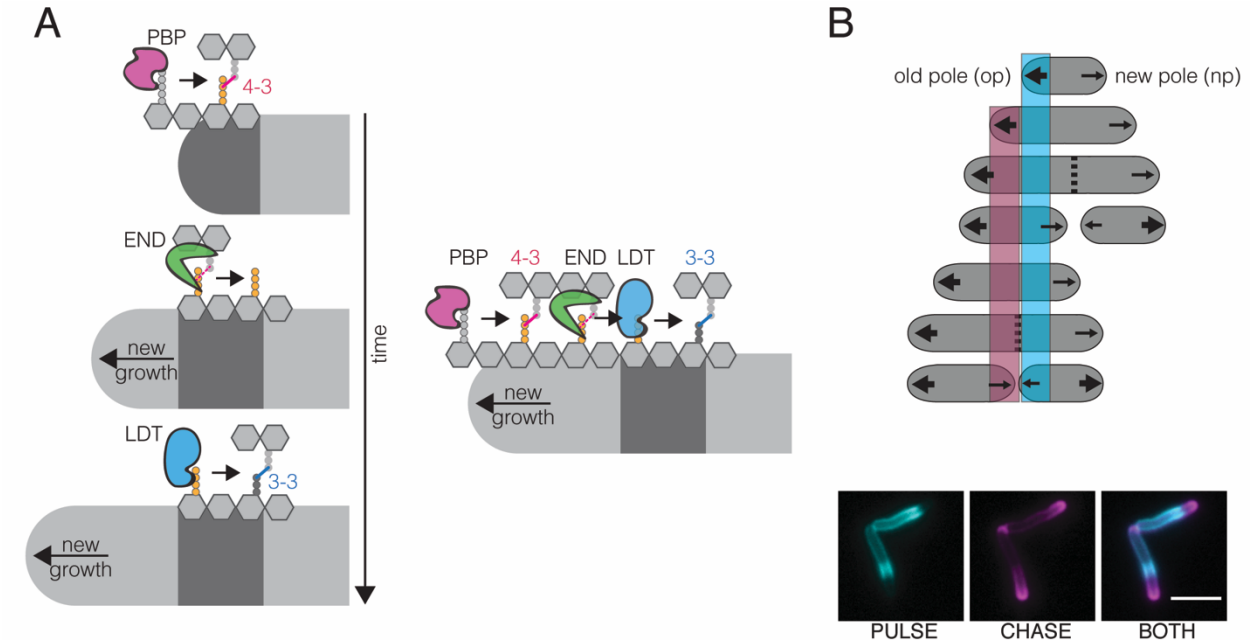

Figure 6: Model for PG enzyme and substrate distribution as governed by polar growth and PG segregation by age. (A) A model for PG age, PG enzyme and crosslink segregation via polar growth in mycobacteria. **(B)** Schematic of PG segregation by age (top). 2-minute FDAA pulse (cyan), 45-minute outgrowth, followed by 2-minute FDAA chase (magenta) in WT Msm cells (bottom). Newest cell wall (magenta), older cell wall (cyan). Scale bar=5μm

388 **Supplementary Materials**
389

390 **Materials and Methods**

391 Bacterial strains and culture conditions

392 Unless otherwise stated, *Mycobacterium smegmatis* (mc^{2}155) was grown shaking at
393 37°C in liquid 7H9 media consisting of Middlebrook 7H9 salts with 0.2% glycerol,
394 0.85g/L NaCl, ADC (5g/L albumin, 2g/L dextrose, 0.003g/L catalase), and 0.05% Tween
395 80 and plated on LB agar. *Mycobacterium tuberculosis* (H37Rv) was grown in liquid
396 7H9 with OADC (oleic acid, albumin, dextrose, catalase) with 0.2% glycerol and 0.05%
397 Tween 80. Antibiotic selection for *M. smegmatis* and *M. tuberculosis* were done at the
398 following concentrations in broth and on agar: 25μg/mL kanamycin, 50μg/mL
399 hygromycin, 20μg/mL zeocin and 20μg/mL nourseothricin and, twice those
400 concentrations for cloning in *Escherichia coli* (TOP10, XL1-Blue and DH5α).
401

402 Strain construction

403 *M. smegmatis* mc^{2}155 mutants lacking *ldtABECFG* (ΔLDT) was constructed using
404 recombineering to replace endogenous copies with zeocin or hygromycin resistance
405 cassettes flanked by lox sites as previously described (Boutte et al., 2016). Briefly, 500
406 base pairs of upstream and downstream sequence surrounding the gene of interest
407 were amplified via PCR (KOD Xtreme™ Hot Start DNA polymerase (EMD Millipore,
408 Billerica, MA)). These flanking regions were amplified with overlaps to either a zeocin or
409 hygromycin resistance cassette flanked by loxP sites and these pieces were assembled
410 into a deletion construct via isothermal assembly (Gibson et al., 2009). Each deletion

411 cassette was transformed into Msm expressing inducible copies of RecET for
412 recombination (Murphy, Papavinasasundaram, & Sassetti, 2015). Once deletions were
413 verified by PCR using and sequencing, the antibiotic resistance cassettes were
414 removed by the expression of Cre recombinase. The order of deletion construction in
415 the ΔLDT strain was as follows (where arrows represent transformation of a Cre-
416 recombinase plasmid, followed by curing of the Cre-recombinase plasmid as it contains
417 the *sacB* gene for sucrose counter selection on LB supplemented with 10% sucrose,
418 and strain names are listed in parenthesis). This resulted in the removal of antibiotic
419 cassettes flanked by loxP sites:

420 1) mc^{2}155Δ*ldtA*:: zeo^R (KB103)→ mc^{2}155Δ*ldtA*::loxP (KB134)
421 2) mc^{2}155Δ*ldtA::loxP* + Δ*ldtE*:: zeo^R (KB156)
422 3) mc^{2}155Δ*ldtA::loxP* Δ*ldtE*:: zeo^R + Δ*ldtB*:: hyg^R (KB200) → mc^{2}155Δ*ldtA::loxP*
423 Δ*ldtE*::loxP Δ*ldtB*::loxP (KB207)
424 4) mc^{2}155Δ*ldtA::loxP* Δ*ldtE*::loxP Δ*ldtB*::loxP + Δ*ldtC*:: hyg^R (KB209)
425 5)mc^{2}155Δ*ldtA::loxP* Δ*ldtE*::loxP Δ*ldtB*::loxP Δ*ldtC*:: hyg^R Δ*ldtG*:: zeo^R (KB222)→
426 mc^{2}155Δ*ldtA::*loxP Δ*ldtE*::loxP Δ*ldtB*::loxP Δ*ldtC*:: loxP Δ*ldtG*:: loxP (KB241)
427 6) mc^{2}155Δ*ldtA::*loxP Δ*ldtE*::loxP Δ*ldtB*::loxP Δ*ldtC*:: loxP Δ*ldtG*:: loxP Δ*ldtF*:: hyg^R
428 (KB303 referred to as ΔLDT) .
429
430 *M. tuberculosis* H37Rv was transformed with a vector expressing the codon optimized
431 *Photorhabdus luminescens luxABCDE* operon (pMV306hsp+LuxG13 –Addgene
432 #26161)(Andreu et al., 2010). This strain is referred to as Mtb Lux.

433

434 Refer to Supplemental Table 1 for oligonucleotides, and Supplemental Table 2 for a
435 complete strain list.

436

437 ΔLDT complementation plasmid construction

438 To complement ΔLDT we placed a copy of *ldtE* (*MSMEG_0233*) under the constitutive
439 TetO promoter (a UV15 derivative within a pMC1s plasmid that is inducible with
440 anhydrous tetracycline in the presence of a tet-repressor TetR, which the ΔLDT_{comp}
441 strain lacks (Kieser, Boutte, et al., 2015b)) on vector that integrates at the L5 phage
442 integration site of the chromosome of the ΔLDT strain (the vector is marked with
443 kanamycin resistance). A glycine, glycine, serine linker was cloned between *ldtE* and
444 mRFP in this complementation construct.

445

446 PonA1 transpeptidase essentiality L5 allele swapping

447 To test essentiality of transpeptidation by PonA1 in the ΔLDT cells, L5 allele swapping
448 as described in (Kieser, Boutte, et al., 2015b) was performed. The plasmids used in
449 this experiment were previously published in (Kieser, Boutte, et al., 2015b). Briefly, a
450 wild-type copy of PonA1 (TetO driven expression, L5 integrating and kanamycin
451 marked) was transformed into ΔLDT. Then, the endogenous copy of *ponA1* was
452 replaced with zeocin using the above mentioned recombineering technique (amplifying
453 the construct from a previously published deletion mutation of *ponA1*(Kieser, Boutte, et
454 al., 2015b)). Swapping efficiency of either wildtype or transpeptidase mutant PonA1

455 marked with nourseothricin was tested with a transformation into ΔLDT//L5-TetO-ponA1
456 (WT)-kanamycin.
457
458 *M. tuberculosis* minimum inhibitory concentration (MIC) determination
459 Mtb Lux was grown to log phase and diluted to an OD_{600}=0.006 in each well of non-
460 treated 96 well plates (Genessee Scientific) containing 100μL of meropenem (Sigma
461 Aldrich) and/or amoxicillin (Sigma Aldrich) diluted in 7H9+OADC+5μg/mL clavulanate
462 (Sigma Aldrich). Cells were incubated in drug at 37°C shaking for 7 days, 0.002%
463 resazurin (Sigma Aldrich) was added to each well, and the plates were incubated for 24
464 hours before MICs were determined. Pink wells signify metabolic activity and blue
465 signify no metabolic activity. (Kieser, Baranowski, et al., 2015a) Checkerboard MIC
466 plates and fractional inhibitory concentrations were calculated as described in
467 ("Synergism Testing: Broth Microdilution Checkerboard and Broth Macrodilution
468 Methods," 2016).
469
470 *M. tuberculosis* drug killing assays
471 Mtb Lux was grown to log phase (kanamycin 25μg/mL) and diluted in 30mL inkwells
472 (Corning Lifesciences) to an OD_{600}=0.05 in 7H9+OADC+5μg/mL clavulanate with
473 varying concentrations of amoxicillin, meropenem, or both. 100μL of these cultures
474 were pipetted in duplicate into a white 96-well polystyrene plate (Greiner Bio-One) and
475 luminescence was read in a Synergy H1 microplate reader from BioTek Instrumenmts,
476 Inc. using the Gen5 Software (2.02.11 Installation version). The correlation between

477 relative light units (RLU) and colony forming units (CFU) is shown in Msm in Figure 5 –
478 figure supplement 2.
479
480 Fluorescent D-amino acid labeling
481 NADA (3-[7-nitrobenzofurazan]-carboxamide-D-alanine), HADA (3-[7-hydroxycoumarin]-
482 carboxamide-D-alanine) and TADA (3-[5-carboxytetramethylrhodamine]-carboxamide-
483 D-alanine) were synthesized by Tocris following the published procotol (Kuru, Tekkam,
484 Hall, Brun, & Van Nieuwenhze, 2014). To 1mL of exponentially growing cells 0.1mM of
485 FDAA final was added and incubated for 2 minutes before washing in 7H9 twice. For
486 still imaging, after the second wash, cells were fixed in 7H9 + 1% paraformaldehyde
487 before imaging. For pulse chase experiments, cells were stained, washed with 7H9 and
488 allowed to grow out for 40 minutes before being stained with a second dye and imaged.

489 Flow cytometry
490 An *M. smegmatis* transposon library was grown to mid-log phase, and stained with 2
491 µg/mL NADA for 2 minutes. Cells were centrifuged and half of the supernatant was
492 discarded. The pellet was resuspended in the remaining supernatant, passed through a
493 10µm filter and taken to be sorted (FACSAria; Excitation: 488nm; Emission filter:
494 530/30). Two bins were drawn at the lowest and highest staining end of the population,
495 representing 12.5% of the population. 600,000 cells from these bins were sorted into
496 7H9 medium. Half of this was directly plated onto LB agar supplemented with
497 kanamycin to select for cells harboring the transposon. The remaining 300,000 cells
498 were grown out in 7H9 to log phase, stained with FDAA and sorted again to enrich the
499 populations.

500

501 Transposon sequencing, mapping and FDAA flow cytometry enrichment analysis.

502 Genomic DNA (gDNA) was harvested from the sorted transposon library colonies and
503 transposon-gDNA junction libraries were constructed and sequenced using the Illumina
504 Hi-Seq platform (Long et al., 2015). Reads were mapped on the *M. smegmatis* genome,
505 tallied and reads at each TA site for the bins (low/high incorporating sort 1 and 2) were
506 imported into MATLAB and processed by a custom scripts as described in (Rego,
507 Audette, & Rubin, 2017).

508

509 Microscopy

510 Both still imaging and time lapse microscopy were performed on an inverted Nikon TI-E
511 microscope at 60x magnification. Time lapse was done using a CellASIC (B04A plate)
512 with constant liquid 7H9 flow in a 37°C chamber. For turgor experiment (*Figure 2A*),
513 cells were grown in either 7H9 or 7H9 500mM sorbitol overnight, and then switched to
514 either 7H9 with 150mM sorbitol (high osmolar) or to 7H9 alone (iso-osmolar).

515

516 Atomic force microscopy

517 AFM experimentation was conducted as previously(Eskandarian et al., 2017). In short,
518 polydimethylsiloxane (PDMS) – coated coverslips were prepared by spin-coating a
519 mixture of PDMS at a ratio of 15:1 (elastomer:curing agent) with hexane (Sigma
520 296090) at a ratio of 1:10 (PDMS:hexane) (Koschwanez, Carlson, & Meldrum, 2009;
521 Thangawng, Ruoff, Swartz, & Glucksberg, 2007). A 50 µl filtered (0.5 µm pore size
522 PVDF filter – Millipore) aliquot of bacteria grown to mid-exponential phase and

523 concentrated from 2-5 ml of culture was deposited onto the hydrophobic surface of a
524 PDMS-coated coverslip and incubated for ~20 min to increase surface interactions
525 between bacteria and the coverslip. 7H9 medium (~3 ml) was supplied to the sample
526 so as to immerse the bacterial sample and the AFM cantilever in fluid. The AFM
527 imaging mode, Peak Force QNM, was used to image bacteria with a Nanoscope 5
528 controller (Veeco Metrology) at a scan rate of 0.5 Hz and a maximum Z-range of 12 μm.
529 A ScanAsyst fluid cantilever (Bruker) was used. Height, peak force error, DMT
530 modulus, and log DMT modulus were recorded for all scanned images in the trace and
531 retrace directions. Images were processed using Gwyddion (Department of
532 Nanometrology, Czech Metrology Institute). ImageJ was used for extracting bacterial
533 cell profiles in a tabular form.
534
535 Correlated optical fluorescence and AFM
536 Correlated optical fluorescence and AFM images were acquired as described
537 (Eskandarian et al., 2017). Briefly, optical fluorescence images were acquired with an
538 electron-multiplying charge-coupled device (EMCCD) iXon Ultra 897 camera (Andor)
539 mounted on an IX81 inverted optical microscope (Olympus) equipped with an
540 UPLFLN100XO2PH x100 oil immersion objective (Olympus). Transmitted light
541 illumination was provided by a 12V/100W AHS-LAMP halogen lamp. An U-MGFPHQ
542 fluorescence filter cube for GFP with HQ-Ion-coated filters was used to detect GFP
543 fluorescence. The AFM was mounted on top of the inverted microscope, and images
544 were acquired with a Dimension Icon scan head (Bruker) using ScanAsyst fluid
545 cantilevers (Bruker) with a nominal spring constant of 0.7 N m^{-1} in Peak Force QNM

546 mode at a force setpoint ~1nN and typical scan rates of 0.5 Hz. Indentation on the cell
547 surface was estimated to be ~10 nm in the Z-axis. Optical fluorescence microscopy
548 was used to identify Wag31-GFP puncta expressed in a wild-type background(Dhar et
549 al., 2013) in order to distinguish them from cells of the ΔLDT mutant strains.
550

551 Calculating cell surface rigidity

552 A cell profile was extracted from AFM Height and DMT Modulus image channels as
553 sequentially connected linear segments following the midline of an individual cell. A
554 background correction was conducted to by dividing the DMT modulus values of the cell
555 surface by the mean value of the PDMS surface and rescaled to compare the cell
556 surface rigidity between individual cells from different experiments. The DMT modulus
557 reflects the elastic modulus (stress-strain relationship) for each cross-sectional
558 increment along the cell length.
559

560 Analysis of fluorescent protein distribution

561 Using a segmented line, profiles of cells from new to old pole were created at the frame
562 "pre-division" based on physical cell separation of the phase image. A custom FIJI
563 (Schindelin et al., 2012) script was run to extract fluorescence line profiles of each cell
564 and save them as .csv files. These .csv files were imported to Matlab where a custom
565 script was applied to normalize the fluorescence line profile to fractional cell length and
566 to interpolate the fluorescence values to allow for averaging.
567

568 Analysis of cell wall distribution

569 Cells were stained with Alexa488 NHS ester as described previously (Aldridge et al.,
570 2012) and followed via time-lapse microscopy in the CellASIC device. Briefly, 1mL of
571 log phase cells was pelleted at 8,000 rpm for 1 minute and washed with 1mL PBST.
572 The pellet was resuspended in 100uL of PBST and 10uL Alexa Fluor 488 carboxylic
573 acid succinimidyl ester was added for a final concentration of 0.05mg/mL. This was
574 incubated for 3 minutes at room temperature. Stained cells were pelleted for 1 minute at
575 13,000 rpm and washed with 500μL PBST. They were spun again and resuspended in
576 7H9 for outgrowth observation over time in the CellASIC device.
577
578 Analysis of FDAAs
579 Images were analyzed using a combination of Oufti (Paintdakhi et al., 2016) for cell
580 selection followed by custom coded Matlab scripts to plot FDAA fluorescence over
581 normalized cell length, calculate cell length and bin cells by existence of an FDAA
582 labeled septum.
583
584 Generation of transposon libraries
585 *M. smegmatis* cells were transduced at (OD_{600} 1.1-1.7) with *φ*MycoMarT7 phage
586 (temperature sensitive) that has a Kanamycin marked Mariner transposon as previously
587 described (Long et al., 2015). Briefly, mutagenized cells were plated at 37°C on LB
588 plates supplemented with Kanamycin to select for phage transduced cells. Roughly
589 100,000 colonies per library were scraped, and genomic DNA was extracted.
590 Sequencing libraries were generated specifically containing transposon disrupted DNA.
591 Libraries were sequenced on the Illumina platform. Data were analyzed using the

592 TRANSIT pipeline (DeJesus et al., 2015).

593 Peptidoglycan isolation and analysis

594 600mLs of wildtype and ΔLDT cells were grown to log phase and collected via
595 centrifugation at 5000 x g for 10 minutes at 4°C. The resulting pellet was resuspsended
596 in PBS and cells were lysed using a cell disruptor at 35,000psi twice. Lysed cells were
597 boiled in 10% SDS (sodium dodecyl sulfate) for 30 minutes and peptidoglycan was
598 collected via centrifugation at 17,000 x g. Pellets were washed with 0.01% DDM(*n*-
599 Dodecyl β-D-maltoside) to remove SDS and resuspended in 1XPBS + 0.01% DDM. PG
600 was digested with alpha amylase (Sigma A-6380) and alpha chymotrypsin (Amersco
601 0164) overnight. The samples were again boiled in 10% SDS and washed in 0.01%
602 DDM. The resulting pellet was resuspended in 400μL 25mM sodium phosphate pH6,
603 0.5mM MgCl2, 0.01% DDM. 20μL of lysozyme (10mg/mL) and 20μL 5U/μL
604 mutanolysoin (Sigma M9901) were added and incubated overnight at 37°C. Samples
605 were heated at 100°C and centrifuged at 100,000 x g. 128μL of ammonium hydroxide
606 was added and incubated for 5 hours at 37°C. This reaction was neutralized with 122μL
607 of glacial acetic acid. Samples were lyophilized, resuspended in 300μL 0.1% formic acid
608 and subjected to analysis by LC-MS/MS. Peptide fragments were separated with an
609 Agilent Technologies 1200 series HPLC on a Nucleosil C18 column (5μm 100A 4.6 x
610 250mm) at 0.5mL/min flow rate with the following method: Buffer A= 0.1% Formic Acid;
611 Buffer B=0.1% Formic Acid in acetonitrile; 0% B from 0-10 minutes, 0-20% B from 10-
612 100 minutes, 20% B from 100-120 minutes, 20-80% B from 120-130 minutes, 80% B
613 from 130-140 minutes, 80%-0% B from 140- 150minutes, 0% B from 150-170 minutes.

614 MS/MS was conducted in positive ion mode using electrospray ionization on an Agilent
615 Q-TOF (6520).
616
617 Expression and purification of MSMEG_2433 (DacB2)
618 MSMEG_2433 was expressed and purified using a modified method for purification of
619 low molecular weight PBPs that was previously published (Qiao et al., 2014). An N-
620 terminally truncated MSMEG_2433$_{(29-296)}$ was cloned into the pET28b vector for isopropyl
621 β-D-1-thiogalactopyranoside (IPTG) inducible expression in *E. coli* BL21 (DE3). 10mLs
622 of overnight culture grown in LB with Kanamycin (50μg/mL) were diluted 1:100 into 1 L of
623 LB with Kanamycin (50μg/mL) and grown at 37°C until an OD_{600} of 0.5. The culture was
624 cooled to room temperature, induced with 0.5mM IPTG, and shaken at 16°C overnight.
625 Cells were pelleted via centrifugation at 4,000rpm for 20 min at 4°C. The pellet was
626 suspended in 20mL binding buffer (20mM Tris pH 8, 10mM $MgCl_2$, 160mM NaCl, 20mM
627 imidazole) with 1mM phenylmethylsulfonylfluoride (PMSF) and 500μg/mL DNase. Cells
628 were lysed via three passage through a cell disrupter at ≥ 10,000 psi. Lysate was pelleted
629 by ultracentrifugation (90,000 × g, 30 min, 4°C). To the supernatant, 1.0mL washed Ni-
630 NTA resin (Qiagen) was added and the mixture rocked at 4°C for 40 min. After loading
631 onto a gravity column, the resin was washed twice with 10mL wash buffer (20mM Tris pH
632 8, 500mM NaCl, 20mM imidazole, 0.1% Triton X-100). The protein was eluted in 10mL of
633 elution buffer (20 mM Tris pH8, 150mM NaCl, 300mM imidazole, 0.1% reduced Triton X-
634 100) and was concentrated to 1 mL with a 10kD MWCO Amicon Ultra Centrifuge Filter.
635 The final protein concentration was measured by reading absorbance at 280 nm and
636 using the estimated extinction coefficient (29459 $M^{-1}cm^{-1}$) calculate concentration. The

637 protein was diluted to 200μM in elution buffer with 10% glycerol, aliquoted, and stored at
638 -80°C.
639 Proper folding of purified MSMEG_2433$_{(29-296)}$ was tested via Bocillin-FL binding. Briefly,
640 20μM of purified protein was added to penicillin G (100, 1000 U/mL in 20mM K_2HPO_4,
641 140mM NaCl, pH7.5) in a 9μL reaction. The reaction was incubated at 37°C for 1hour.
642 10μM Bocillin-FL was added and incubated at 37°C for 30 minutes. SDS loading dye
643 was added the quench the reaction and samples were loaded onto a 4-20% gel.
644 MSMEG_2433$_{(29-296)}$ bound by Bocillin-FL was imaged using a Typhoon 9400 Variable
645 Mode Imager (GE Healthcare) (Alexa Excitation-488nm Emission-526nm).
646
647 Lipid II extraction.
648 *B. subtilis* Lipid II was extracted as previously published (Qiao et al., 2017).
649
650 SgtB purification.
651 *S. aureus* SgtB was purified as previously published (Rebets et al., 2014).
652
653 Purification of *B. subtilis* PBP1.
654 Purification of *B. subtilis* PBP1 was carried out as previously described (Lebar et al.,
655 2014).
656
657 *In vitro* Lipid II polymerization and crosslinking.
658 20 μM purified BS Lipid II was incubated in reaction buffer (50 mM HEPES pH 7.5, 10
659 mM $CaCl_2$) with either 5 μM PBP1 or 0.33 μM SgtB for 1 hour at room temperature. The

660 enzymes were heat denatured at 95°C for 5 minutes. Purified MSMEG_2433$_{(29-296)}$ was
661 added (20 uM, final) and the reaction was incubated at room temperature for 1 hour.
662 Mutanolysin (1 μL of a 4000 U/mL stock) was added and incubated for 1.5 hours at 37
663 °C (twice). The resulting muropeptides were reduced with 30 μL of $NaBH_4$ (10 mg/mL)
664 for 20 minutes at room temperature with tube flicking every 5 minutes to mix. The pH
665 was adjusted to ~4 using with 20% H_3PO_4 and the resulting product was lyophilized to
666 dryness. The residue was resuspended in 18μL of water and analyzed via LC-MS as
667 previously reported (Welsh et al., 2017).
668

669

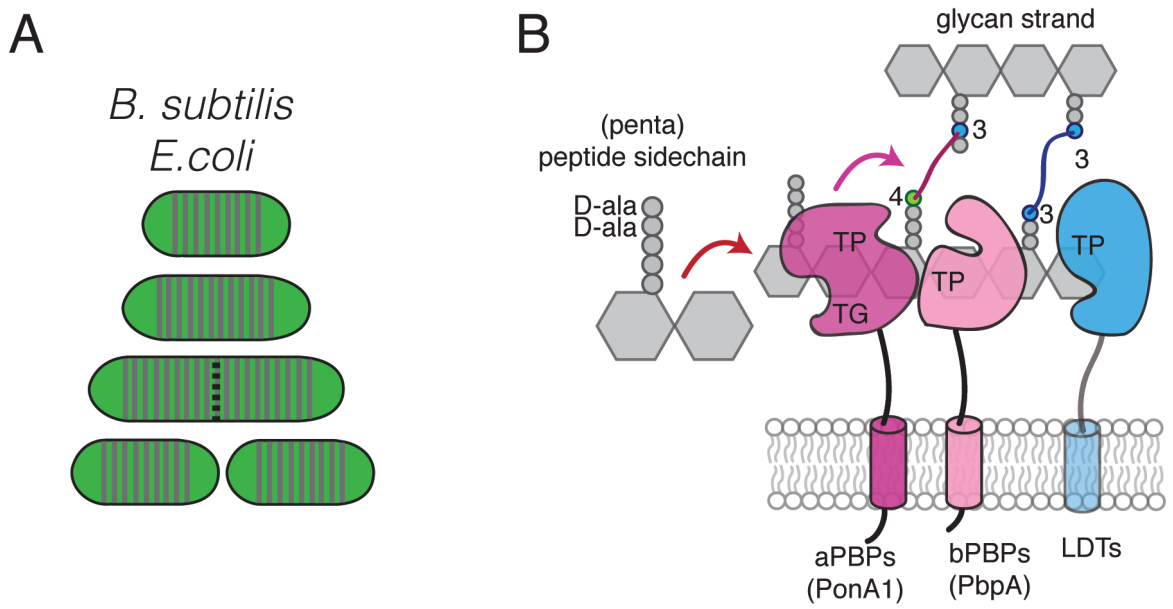

670

671 **Figure 1- figure supplement 1: Peptidoglycan synthesis and FDAA screen**
672 **overview. (A)** *Escherichia coli* and *Bacillus subtilis* lateral cell wall growth. Unlike
673 mycobacteria, *E. coli* and *B. subtilis* insert new cell wall along the lateral cell body, mixing
674 old and new peptidoglycan. Green portion represents old cell wall; grey portion represents
675 new material. **(B)** Cartoon of penicillin binding proteins (PBPs), L,D-transpeptidases
676 (LDTs), and both 4-3 and 3-3 crosslinking. PBPs utilize a pentapeptide substrate found
677 on new peptidoglycan, ending in D-alanine-D-alanine. LDTs utilize a tetrapeptide
678 substrate found on processed peptidoglycan. TP, transpeptidase; TG, transglycosylase

679

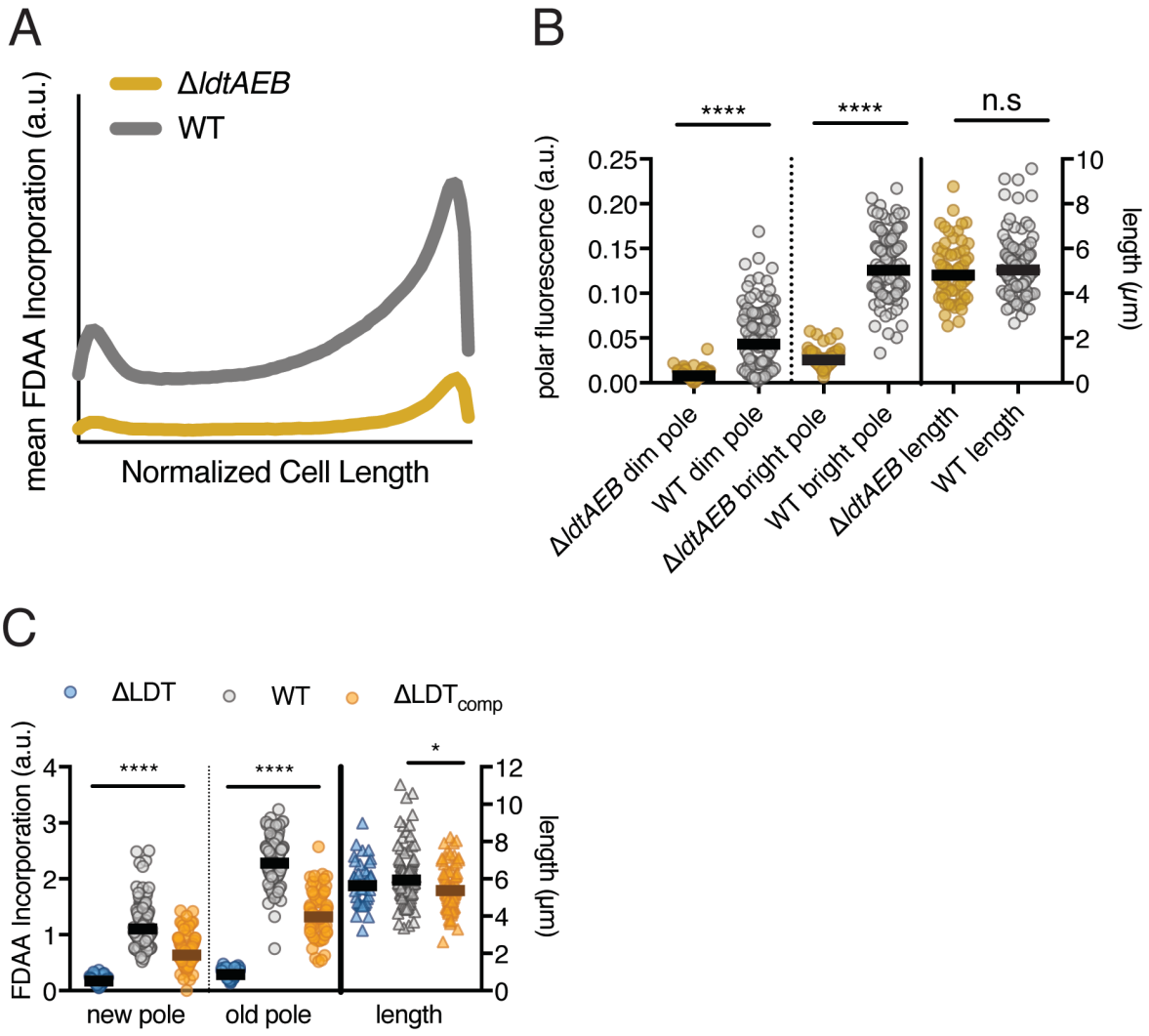

Figure 1- figure supplement 2: Fluorescent D-amino acid screen validation. (A) Mean line profiles (from new to old pole) of FDAA incorporation in log-phase WT (N=97), Δ*ldtABE* (N=64). **(B)** Quantification of FDAA incorporation at cell poles and quantification of cell length. Mann-Whitney U P-Value shown (**** P-Value < 0.0001). **(C)** Quantification of FDAA incorporation at poles and cell lengths of WT, ΔLDT and ΔLDT_{comp} cells shown in Fig. 1E and whose mean incorporation is shown in Fig. 1F.

689

A

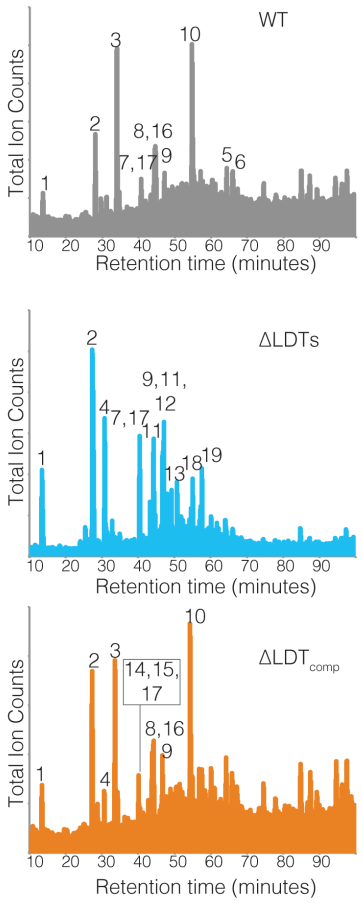

B

PEAK	Tripeptides observed	Description*
1	461.2	
	Tetrapeptides observed	
2	532.3	Tetra (2 NH2)
3	534.2	Tetra (OH)
4	533.2	Tetra (NH2)
	pentapeptides observed	
5	604.3	Penta (OH)
6	602.3	Penta(2 NH2)
	4-3 observed	
7	974.5	4--3 (2 NH2)
8	1045.4	4--4 (4 NH2)
9	1046.5	4--4 (3 NH2)
10	1049.4	4--4
11	975.4	4--3 (NH2)
12	974.3	4--3 (2 NH2)
13	1047.5	4--4 (2 NH2)
	3-3 observed	
14	974.4	4--3 (4 NH2)
15	904.4	3--3 (3 NH2)
16	975.5	4--3 (3 NH2)
	Tripeptide(anhydrous)	
17	865.4	
	4--4--4	
18	1559.7	
19	1560.0	

C

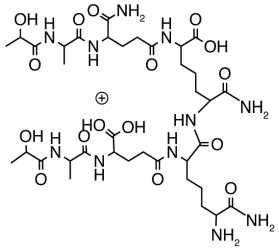

3-3 crosslink (tripeptide-tripeptide)
m/z: 904.44 (100.0%), 905.44 (38.9%), 906.44 (7.4%), 905.43 (4.1%), 906.44 (3.3%), 906.44 (1.6%), 907.44 (1.3%)

D

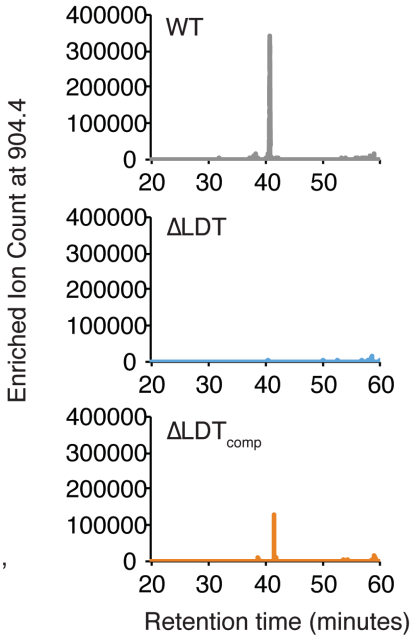

690 **Figure 1- figure supplement 3: 3-3 crosslinks are not detectable in ΔLDT cells. (A)**
691 Total ion chromatograms of WT, ΔLDT and ΔLDT$_{comp}$ peptidoglycan. **(B)** Table of

692 muropeptide masses (Da) observed in (S3A). The molecular weight difference by one of
693 the identified peptides is due to differential amidation. The descriptions include the
694 peptide lengths in the crosslink (4= tetra-, 3= tri- peptide) and the following parenthesis
695 specifies the number of amidation in the species according to mass. **(C)** Structure of a
696 representative 3-3 crosslink with a m/z=904.4. **(D)** Extracted ion chromatograms from
697 WT, ΔLDT and ΔLDT_{comp} for a representative 3-3 crosslink with a m/z=904.4.
698

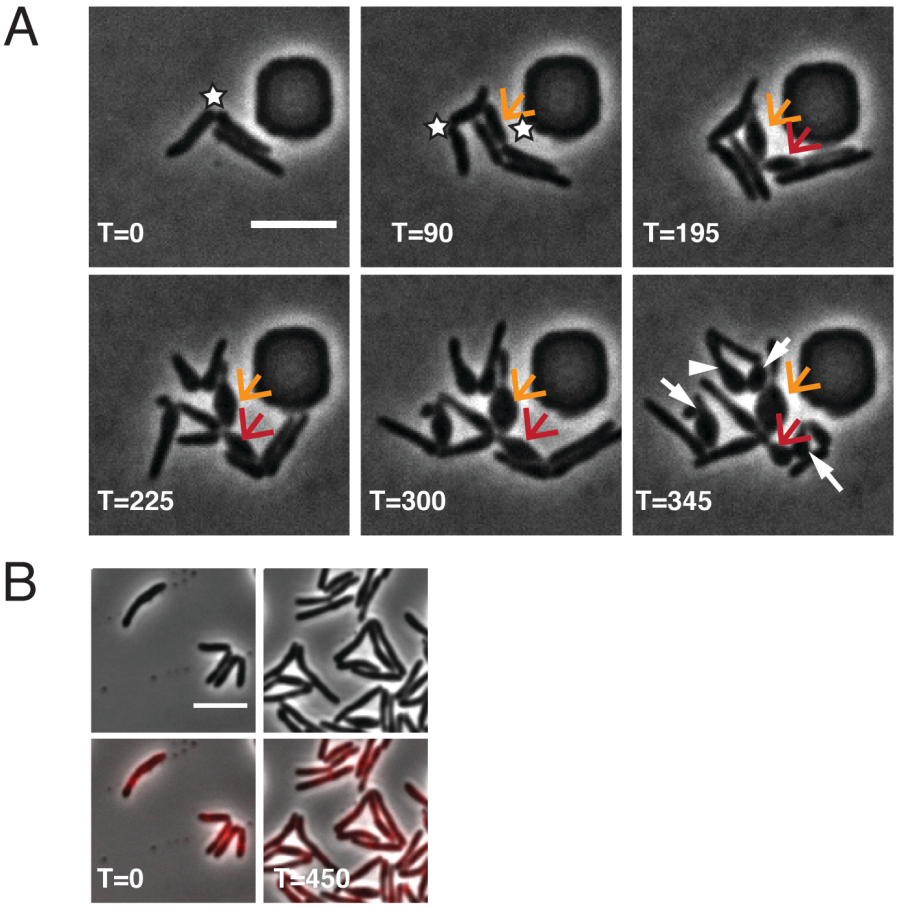

Figure 2- figure supplement 1: ΔLDT cell morphological characteristics. (A) Time-lapse microscopy montage of ΔLDT cells. The white stars mark new poles. The orange arrow points to the first new pole daughter cell of this series. The red arrow indicates the second resulting new pole daughter cell. In the last frame, white arrows point to all new pole daughter cells (besides the orange arrow and red arrow). **(B)** Time-lapse microscopy montage of ΔLDT_{comp} cells expressing LdtE-mRFP.
All scale bars=5μm

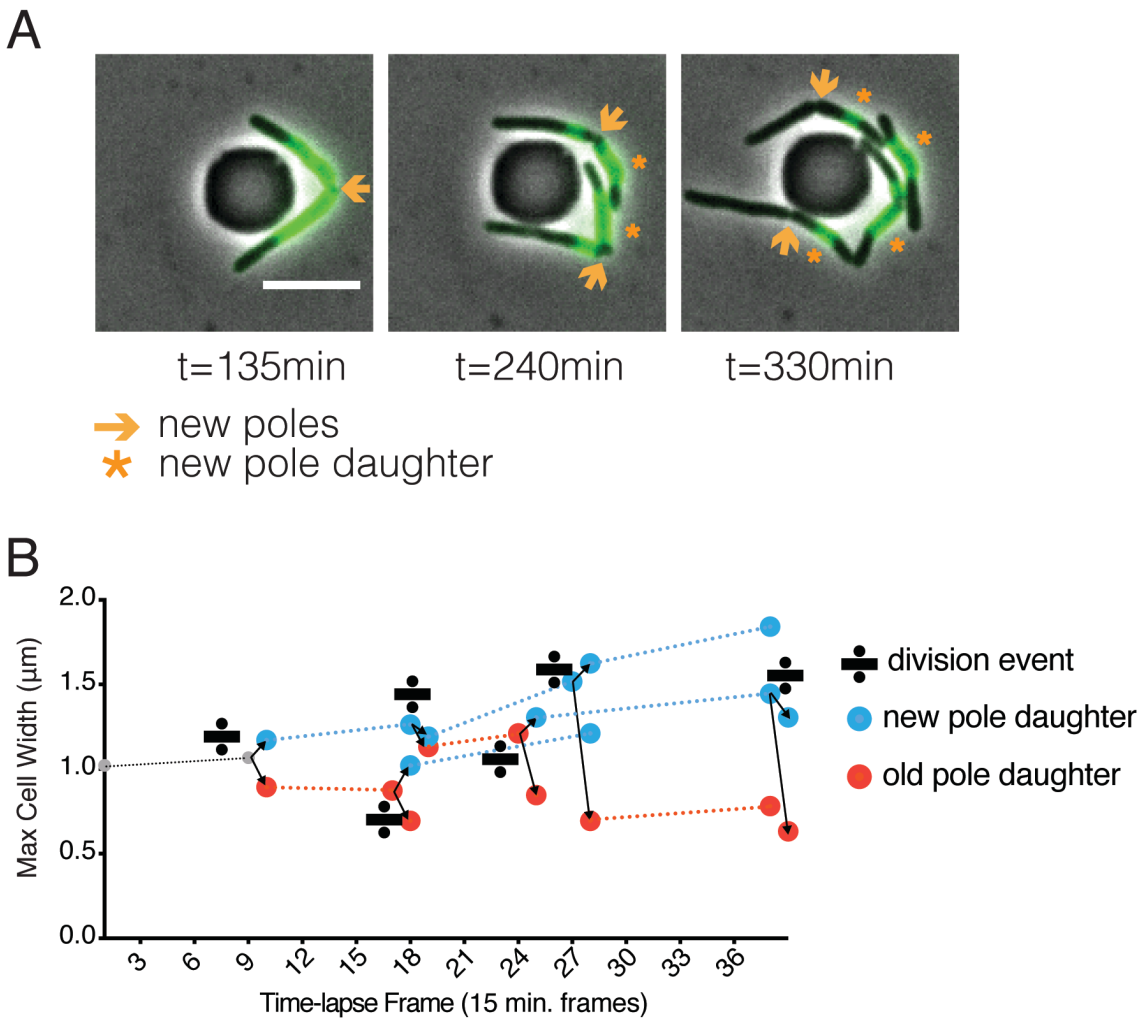

Figure 2- figure supplement 2: Inheritance of old cell wall and occurrence of blebs in new pole daughter cells. (A) WT Msm stained with Alexa Fluor™ 488 NHS ester, washed and visualized over time. New material is unstained, old material is stained green. Orange arrows indicate a new pole. Orange stars mark new pole daughter cells. All scale bars=5µm **(B)** Maximum cell width of ΔLDT cell lineages over time. Width of new pole daughters = blue circle; width of old pole daughters = orange circle. Division signs denote a division event. At each division, there are two arrows from the dividing cell leading to the resulting new and old pole daughter cell widths (blue and orange respectively).

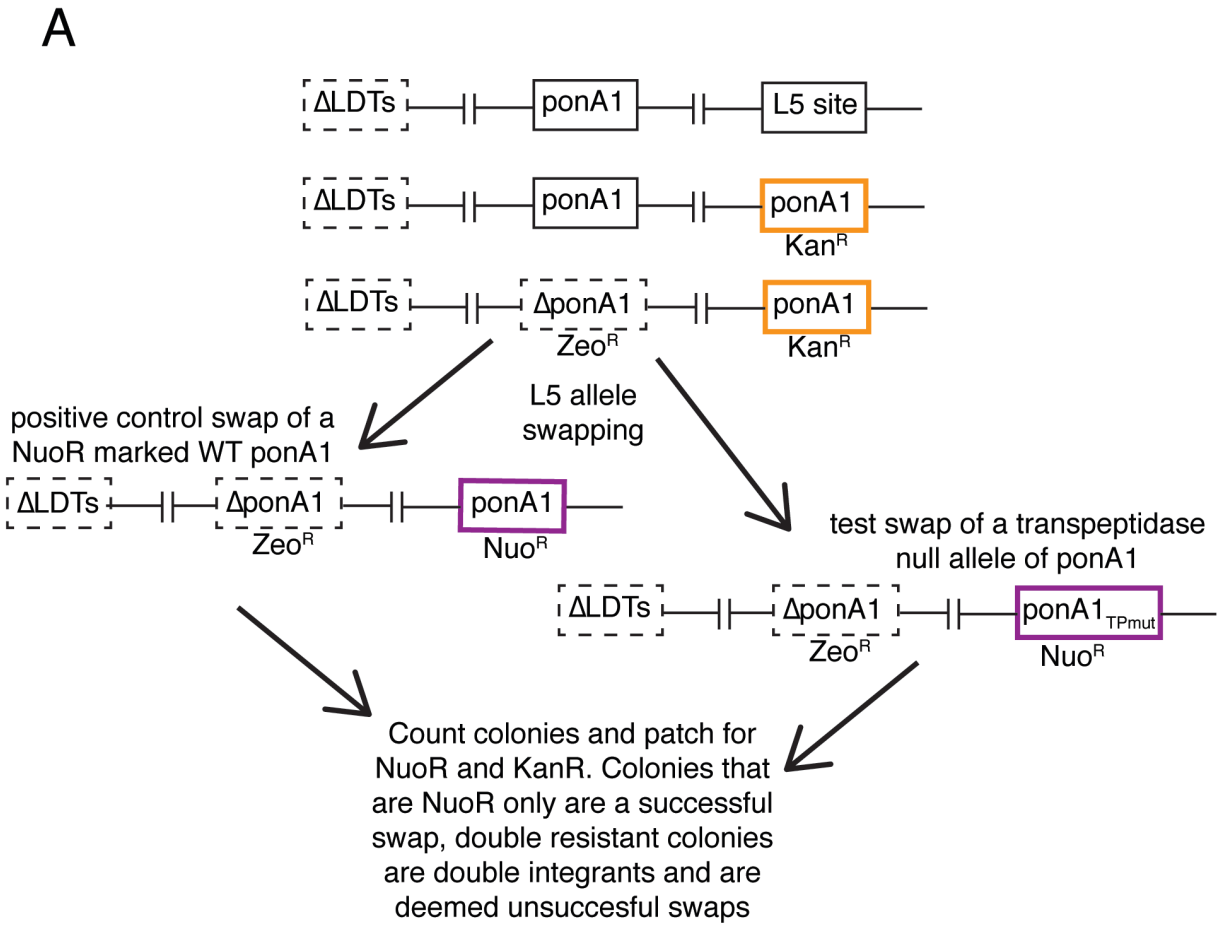

Figure 3- figure supplement 1: L5 allele swapping to test essentiality of PonA1's ability to form 4-3 crosslinks (transpeptidation). (A) Schematic of L5 allele swapping experiment. Adapted from (Kieser, Boutte, et al., 2015b).

726

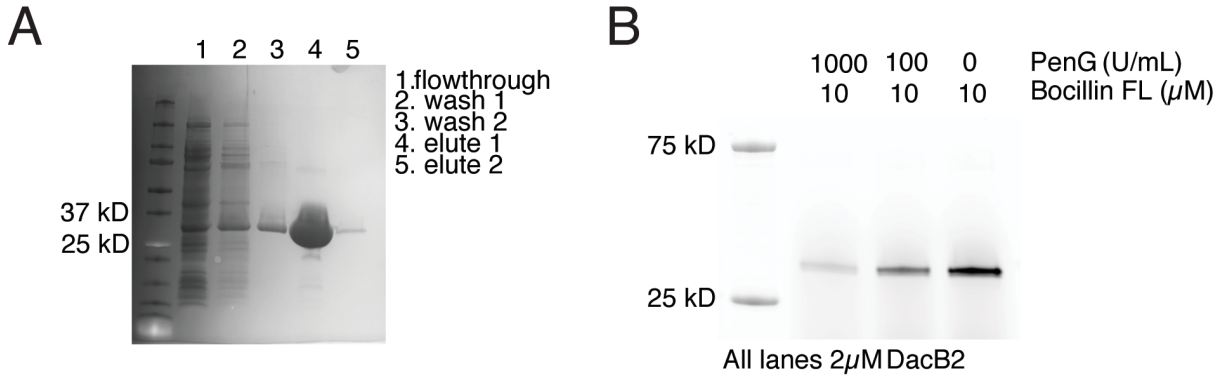

727

728 **Figure 4- figure supplement 1: MSMEG_2433 (DacB2) functions as a D,D-**
729 **carboxypeptidase and D,D-endopeptidase *in vitro*. (A)** Coomassie-stained gel of
730 purified His_6-DacB2. **(B)** Bocillin-FL and Penicillin G binding assay of purified DacB2.

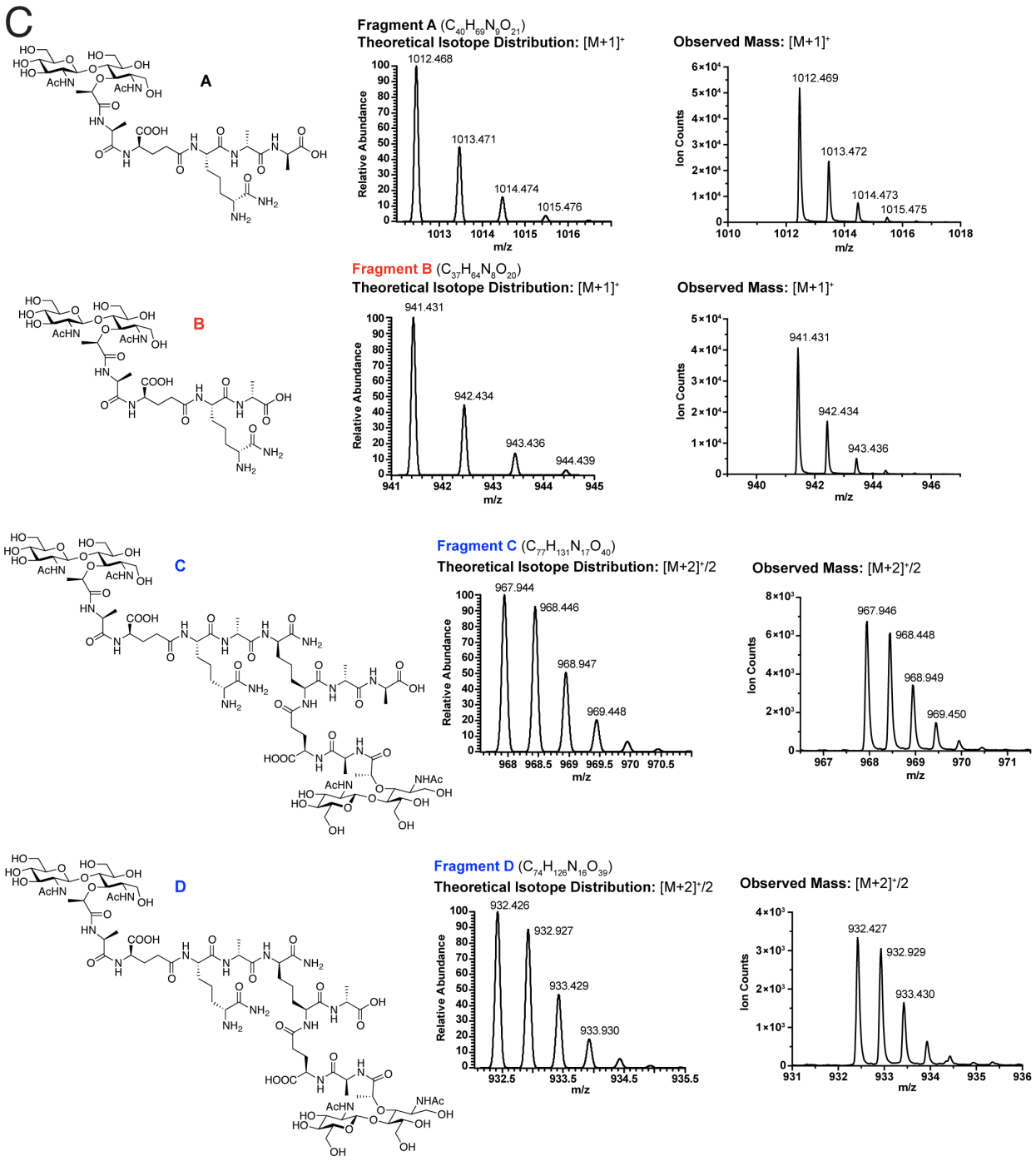

Figure 4- figure supplement 1 (continued): MSMEG_2433 (DacB2) functions as a D,D-carboxypeptidase and D,D-endopeptidase *in vitro*. (C) Mass spectra of the reaction products of DacB2 digestion reactions.

A

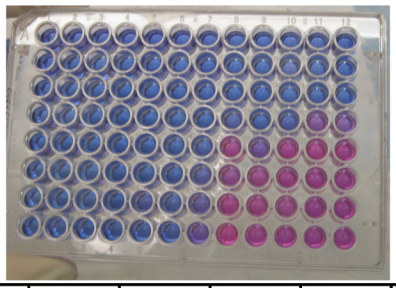

	1	2	3	4	5	6	7	8	9	10	11	12
	10.00	10.00	10.00	10.00	10.00	10.00	10.00	10.00	10.00	10.00	10.00	
A	10.00	5.00	2.50	1.25	0.63	0.31	0.16	0.08	0.04	0.02	0.01	
	5.00	5.00	5.00	5.00	5.00	5.00	5.00	5.00	5.00	5.00	5.00	
B	10.00	5.00	2.50	1.25	0.63	0.31	0.16	0.08	0.04	0.02	0.01	
	2.50	2.50	2.50	2.50	2.50	2.50	2.50	2.50	2.50	2.50	2.50	
C	10.00	5.00	2.50	1.25	0.63	0.31	0.16	0.08	0.04	0.02	0.01	
	1.25	1.25	1.25	1.25	1.25	1.25	1.25	1.25	1.25	1.25	1.25	
D	10.00	5.00	2.50	1.25	0.63	0.31	0.16	0.08	0.04	0.02	0.01	
	0.63	0.63	0.63	0.63	0.63	0.63	0.63	0.63	0.63	0.63	0.63	
E	10.00	5.00	2.50	1.25	0.63	0.31	0.16	0.08	0.04	0.02	0.01	
	0.31	0.31	0.31	0.31	0.31	0.31	**0.31**	0.31	0.31	0.31	0.31	
F	10.00	5.00	2.50	1.25	0.63	0.31	**0.16**	0.08	0.04	0.02	0.01	
	0.16	0.16	0.16	0.16	0.16	0.16	0.16	0.16	0.16	0.16	0.16	
G	10.00	5.00	2.50	1.25	0.63	0.31	0.16	0.08	0.04	0.02	0.01	
	0.08	0.08	0.08	0.08	0.08	0.08	0.08	0.08	0.08	0.08	0.08	
H	10.00	5.00	2.50	1.25	0.63	0.31	0.16	0.08	0.04	0.02	0.01	

B

	1	2	3	4	5	6	7	8	9	10	11	12	
A	40.00	20.00	10.00	5.00	2.50	1.25	**0.63**	0.31	0.16	0.08	0.04	0.02	
													amoxicillin
B	40.00	20.00	10.00	5.00	2.50	1.25	**0.63**	0.31	0.16	0.08	0.04	0.02	
C	40.00	20.00	10.00	5.00	2.50	**1.25**	0.63	0.31	0.16	0.08	0.04	0.02	
													meropenem
D	40.00	20.00	10.00	5.00	2.50	**1.25**	0.63	0.31	0.16	0.08	0.04	0.02	

Figure 5- figure supplement 1: Minimum inhibitory concentration (MIC) of amoxicillin or meropenem alone or in combination against *Mycobacterium*

742 ***tuberculosis*. (A)** Resazurin MIC plate and dilution matrix of amoxicillin and meropenem
743 in combination in a checkerboard MIC plate. The table below shows the concentration of
744 each drug per well in μg/mL. The concentration of meropenem is in black text and the
745 concentration of amoxicillin is in red text in each well. **(B)** Dilution matrix of amoxicillin or
746 meropenem (alone). The concentrations of drugs are shown in the table. Pink indicates
747 metabolically active cells, blue indicates not metabolically active. In both single drug and
748 checkerboard MIC plates, 5μg/mL clavulanate was used.
749

750

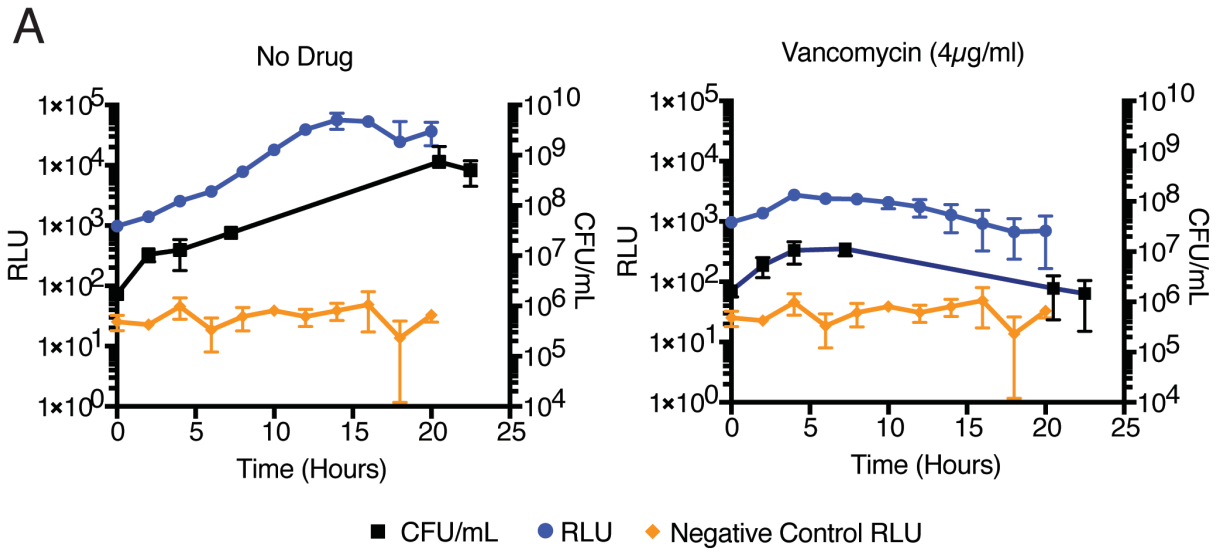

751

752 **Figure 5- figure supplement 2: Light production (RLU) correlated to colony forming**
753 **units (CFU) in mycobacterial cells expressing *luxABCDE* in drug treatment. (A)**
754 *Mycobacterium smegmatis* colony forming units (CFU) and luminescence (RLU) during
755 drug treatment.

756

Video captions

Figure 2-video1- Time-lapse of ΔLDT cells in iso-osmolar media.
This video corresponds to Figure 2A (top). This is a time-lapse microscopy video of ΔLDT Msm cells growing in 7H9 (iso-osmolar) media. Frames are 15 minutes apart, and the video is 5 frames/second.

Figure 2-video2- Time-lapse of ΔLDT cells in high-osmolar media.
This video corresponds to Figure 2A (bottom). This is a time-lapse microscopy video of ΔLDT Msm cells growing in 7H9 +150mM sorbitol (high-osmolar) media. Frames are 15 minutes apart, and the video is 5 frames/second.

Figure 4-video1- Time-lapse of ponA1-RFP.
This video corresponds to Figure 4A,B. This is a time-lapse microscopy video of Msm cells expressing ponA1-RFP growing in 7H9 media. Frames are 15 minutes apart, and the video is 5 frames/second.

Figure 4-video2- Time-lapse of ldtE-mRFP.
This video corresponds to Figure 4A,B. This is a time-lapse microscopy video of Msm cells expressing ldtE-mRFP growing in 7H9 media. Frames are 15 minutes apart, and the video is 5 frames/second.

Figure 4-video3- Time-lapse of dacB2-mRFP.
This video corresponds to Figure 4A,B. This is a time-lapse microscopy video of Msm cells expressing dacB2-mRFP growing in 7H9 media. Frames are 15 minutes apart, and the video is 5 frames/second.

787
788 **Supplementary table 1: List of Primers**
789

Primer description	Primer Sequence	5' or 3' features	Primer #
MSMEG_3528 (ldtA) upstream flanking region FOR	CGTTGTAAAACGACGGCCAGTGATGGCGGGCGTGATCTGGAATCTCT	pUC57 overlap	208
MSMEG_3528 (ldtA) upstream flanking region REV	ACCCAACTTAATCGCCTTGCAGCTCTTCCAGTGTAGGTTGTCGAAACG	Zeo cassette overlap	209
MSMEG_3528 (ldtA) downstream flanking region FOR	TAATCATGGTCATAGCTGTTTTCATCGTGCAGGCGTGACGTGCAG	Zeo cassette overlap	210
MSMEG_3528 (ldtA) downstream flanking region REV	CAGTCGACGGGCCCGGGATCCGCGGTGGTGCCCTTGGTGATGGTC	pUC57 overlap	211
MSMEG_0233 (ldtE) upstream flanking region FOR	CGTTGTAAAACGACGGCCAGTGGCTGTCCGCCCAGCCCCGGGCC	pUC57 overlap	220
MSMEG_0233 (ldtE) upstream flanking region REV	CCAACTTAATCGCCTTGCAGCGTGGTACCTCCAGAGCACAACTG	Zeo cassette overlap	221
MSMEG_0233 (ldtE) downstream flanking region FOR	GTAATCATGGTCATAGCTGTTTCCGGACGTCATACGAAGAACCCCC	Zeo cassette overlap	222
MSMEG_0233 (ldtE) downstream flanking region REV	GCAGTCGACGGGCCCGGGATCTGGACCGACGCCGACCGCACCG	pUC57 overlap	223
MSMEG_4745 (ldtB) upstream flanking region FOR	GGTCGAGATGCTCCTGGAAGAGGCCG		444

MSMEG_4745 (ldtB) upstream flanking region REV	GAGCTCCAATTCGCCCTACGTCGTTACCTGCCCCATCACG	hyg cassette overlap	445
MSMEG_4745 (ldtB) downstream flanking region FOR	GTACCTCGAGTCTAGAAGTAGCGCTATCGCACCGCGCGGTCCAG	hyg cassette overlap	446
MSMEG_4745 (ldtB) downstream flanking region REV	CGACCCGGCCCGTCACAAGGACACCGAAC		447
MSMEG_0929 (ldtC) upstream flanking region FOR	CGTTGTAAAACGACGGCCAGTGAACTGGCGACGGCGCTGGGCGTGG	pUC57 overlap	216
MSMEG_0929 (ldtC) upstream flanking region REV	TGGAGCTCCAATTCGCCCTAGTGGATCTAGGGTACCGACAGCACGC	hyg cassette overlap	448
MSMEG_0929 (ldtC) downstream flanking region FOR	GGTACCTCGAGTCTAGAAGTAGTCCGGCGGCTAGGTCCGGCGGTTGAAG	hyg cassette overlap	449
MSMEG_0929 (ldtC) downstream flanking region REV	CAGTCGACGGGCCCGGGATCCCAAGGGACTCGCGCCGGTCTCC	pUC57 overlap	219
MSMEG_0929 (ldtC) upstream flanking region FOR	GGCTCGTTCTTCACCAACC		507
MSMEG_0929 (ldtC) downstream flanking region REV	CTGCCCAAGCTCATCGAC		508
MSMEG_0674 (ldtG) upstream flanking region FOR	GTTGTAAAACGACGGCCAGTGCGGCGTCGACCTCCCGGCCGGGTC	pUC57 overlap	228

MSMEG_0674 (ldtG) upstream flanking region REV	GTGGAGCTCCAATTCGCCCTAGCGCATTGGCTTCCGATTTCCCTCG	hyg cassette overlap	454
MSMEG_0674 (ldtG) downstream flanking region FOR	CGGTACCTCGAGTCTAGAAGTACGCCGACGTGTATGCCCACCCCCGCG	hyg cassette overlap	455
MSMEG_0674 (ldtG) downstream flanking region REV	GCAGTCGACGGGCCCGGGATCGCCTGCGCCCGCGGGAGCGCCTGCC	pUC57 overlap	231
MSMEG_0674 (ldtG) upstream flanking region FOR	GCATCTGAGTTTCGGCAAG		513
MSMEG_0674 (ldtG) downstream flanking region REV	CAACTACCCCGCAGTTGAAT		514
MSMEG_1322 (ldtF) upstream flanking region FOR	GTTGTAAAACGACGGCCAGTGCGAGGTAAGGGTCTCGACGGTTTCT	pUC57 overlap	224
MSMEG_1322 (ldtF) upstream flanking region REV	GTGGAGCTCCAATTCGCCCTATCCAATGTGCTTCGGCGAAAGCCAGTTTG	hyg cassette overlap	452
MSMEG_1322 (ldtF) downstream flanking region FOR	GTACCTCGAGTCTAGAAGTAGTTCCCCCCGGCCCACATATGTCTGGACG	hyg cassette overlap	453
MSMEG_1322 (ldtF) downstream flanking region REV	GCAGTCGACGGGCCCGGGATCCACGACAACGCCAGCGCGAT	pUC57 overlap	227
MSMEG_1322 (ldtF) upstream flanking region FOR	GGTCGACGACGAACTGGT		511
MSMEG_1322 (ldtF) downstream	AACGGCACGTACATCAGGAC		512

flanking region REV			
MSMEG_0233 (ldtE) FOR with TetO overlap (vector)	CATGCTTAATTAAGAAGGAGATATACAATGCCGAAATCGGCAAAACGCAG		323A
MSMEG_0233 (ldtE) REV (no stop codon) with ser-ser-gly linker	GATGACGTCCTCGGAGGAGGCCGAGCCGCCGAACATCTGCCAGTCGGATG		351
mRFP FOR with ser-ser-gly linker	CATCCGACTGGCAGATGTTCGGCGGCTCGGCCTCCTCCGAGGACGTCATC		352
mRFP REV with vector overlap	GTCCCCAATTAATTAGCTAAGTGATGGTGATGGTGATGACAGGCG		353
MSMEG_2433 (dacB2) FOR (first 27 amino acids truncated)	GGCCTGGTGCCGCGCGGCAGCCATCGCGCGGACGCCGACATCCAG	with 5' overlaps to pet28b cut with NdeI	662
MSMEG_2433 (dacB2) REV	GCTGTCCACCAGTCATGCTAGCCATCAGAGCGCCCCGATGCTCG	with 3' overlaps to pet28b cut with NdeI	663

790
791

792 **Supplementary Table 2: List of Strains**

793

Strain	Description	Primers
KB134	mc2155Δ*ldtA*::loxP	208/209; 210/211
KB156	mc2155Δ*ldtA*::loxP + Δ*ldtE*:: zeoR	220/221; 222/223
KB200	mc2155Δ*ldtA*::loxP Δ*ldtE*:: zeoR + Δ*ldtB*:: hygR	444/445; 446/447
KB209	mc2155Δ*ldtA*::loxP Δ*ldtE*::loxP Δ*ldtB*::loxP + Δ*ldtC*:: hygR	216/448; 449/219 (create original hyg KO) but used 507/508; (amplify KO from strain within the flanks)
KB222	mc2155Δ*ldtA*::loxP Δ*ldtE*::loxP Δ*ldtB*::loxP Δ*ldtC*:: hygR Δ*ldtG*:: zeoR	228/454; 455/231 (create original hyg KO) but used 513/514; (amplify KO from strain within the flanks)
KB303 (ΔLDT)	mc2155Δ*ldtA*::loxP Δ*ldtE*::loxP Δ*ldtB*::loxP Δ*ldtC*:: loxP Δ*ldtG*:: loxP Δ*ldtF*:: hygR	224/452; 453/227 (create hyg KO) but used 511/512 (amplify KO from strain or gibson)
KB302	pTetO-ldtE(MSMEG_0233)-linker-mRFP in CT94 XH (XL1-Blue)	323A/351; 352/353
KB316 (ΔLDTcomp)	[mc2155ΔldtA::loxP ΔldtE::loxP ΔldtB::loxP ΔldtC:: loxP ΔldtG:: loxP ΔldtF:: hygR] + KB302	
KB428	*E.coli* BL21 + pet28b (dacB2)	662/663

794

795

796 **Supplemental Table 3: FDAA FACs screen data used for Figure 1D**
797
798 **Supplemental Table 4: ∆LDT Tnseq data used for Figure 3A**
799 Below are the column names with a brief description-
800 Orf - ID of gene
801 Name - name of gene
802 Desc - annotation of gene
803 Sites - number of TA sites in gene
804 Mean Ctrl - mean insertion count averaged over TA sites and replicates for wildtype
805 strain (mc^2155)
806 Mean Exp - mean insertion count averaged over TA sites and replicates for knockout
807 strain (ΔLDT)
808 log2FC - log-fold-change, log2(meanExp/meanCtl)
809 Sum Ctrl - sum of insertion counts over TA sites and replicates for wildtype strain
810 (mc^2155)
811 Sum Exp - sum of insertion counts over TA sites and replicates for knockout strain
812 (ΔLDT)
813 Delta Sum - difference of sums (sumExp-sumCtl)
814 p-value - probability of null hypothesis (i.e. no significant difference between strains)
815 estimated from resampling distribution
816 Adj. p-value - p-values after applying Benjamini-Hochberg correction for multiple tests
817
818
819
820
821
822

References:

Aldridge, B. B., Fernandez-Suarez, M., Heller, D., Ambravaneswaran, V., Irimia, D., Toner, M., & Fortune, S. M. (2012). Asymmetry and aging of mycobacterial cells lead to variable growth and antibiotic susceptibility. *Science*, *335*(6064), 100–104. http://doi.org/10.1126/science.1216166

Andreu, N., Fletcher, T., Krishnan, N., Wiles, S., & Robertson, B. D. (2012). Rapid measurement of antituberculosis drug activity in vitro and in macrophages using bioluminescence. *The Journal of Antimicrobial Chemotherapy*, *67*(2), 404–414. http://doi.org/10.1093/jac/dkr472

Andreu, N., Zelmer, A., Fletcher, T., Elkington, P. T., Ward, T. H., Ripoll, J., et al. (2010). Optimisation of bioluminescent reporters for use with mycobacteria. *PLoS ONE*, *5*(5), e10777. http://doi.org/10.1371/journal.pone.0010777

Bansal, A., Kar, D., Murugan, R. A., Mallick, S., Dutta, M., Pandey, S. D., et al. (2015). A putative low-molecular-mass penicillin-binding protein (PBP) of Mycobacterium smegmatis exhibits prominent physiological characteristics of DD-carboxypeptidase and beta-lactamase. *Microbiology (Reading, England)*, *161*(Pt 5), 1081–1091. http://doi.org/10.1099/mic.0.000074

Botella, H., Yang, G., Ouerfelli, O., Ehrt, S., Nathan, C. F., & Vaubourgeix, J. (2017). Distinct Spatiotemporal Dynamics of Peptidoglycan Synthesis between Mycobacterium smegmatis and Mycobacterium tuberculosis. *mBio*, *8*(5), e01183–17. http://doi.org/10.1128/mBio.01183-17

Boutte, C. C., Baer, C. E., Papavinasasundaram, K., Liu, W., Chase, M. R., Meniche, X., et al. (2016). A cytoplasmic peptidoglycan amidase homologue controls mycobacterial cell wall synthesis. *eLife*, *5*, a021113. http://doi.org/10.7554/eLife.14590

Böth, D., Schneider, G., & Schnell, R. (2011). Peptidoglycan remodeling in Mycobacterium tuberculosis: comparison of structures and catalytic activities of RipA and RipB. *Journal of Molecular Biology*, *413*(1), 247–260. http://doi.org/10.1016/j.jmb.2011.08.014

Brown, P. J. B., de Pedro, M. A., Kysela, D. T., Van der Henst, C., Kim, J., De Bolle, X., et al. (2012). Polar growth in the Alphaproteobacterial order Rhizobiales. *Proceedings of the National Academy of Sciences of the United States of America*, *109*(5), 1697–1701. http://doi.org/10.1073/pnas.1114476109

Cameron, T. A., Zupan, J. R., & Zambryski, P. C. (2015). The essential features and modes of bacterial polar growth. *Trends in Microbiology*, *23*(6), 347–353. http://doi.org/10.1016/j.tim.2015.01.003

Cava, F., de Pedro, M. A., Lam, H., Davis, B. M., & Waldor, M. K. (2011). Distinct pathways for modification of the bacterial cell wall by non-canonical D-amino acids. *The EMBO Journal*, *30*(16), 3442–3453. http://doi.org/10.1038/emboj.2011.246

DeJesus, M. A., Ambadipudi, C., Baker, R., Sassetti, C., & Ioerger, T. R. (2015). TRANSIT - A Software Tool for Himar1 TnSeq Analysis. *PLoS Computational Biology*, *11*(10), e1004401–17. http://doi.org/10.1371/journal.pcbi.1004401

Dhar, N., Bousbaine, D., Wakamoto, Y., McKinney, J. D., & Santi, I. (2013). Single-cell dynamics of the chromosome replication and cell division cycles in mycobacteria.

Nature Communications, *4*, 1–10. http://doi.org/10.1038/ncomms3470
Diacon, A. H., van der Merwe, L., Barnard, M., Groote-Bidlingmaier, von, F., Lange, C., García-Basteiro, A. L., et al. (2016). β-Lactams against Tuberculosis--New Trick for an Old Dog? *The New England Journal of Medicine*, *375*(4), 393–394. http://doi.org/10.1056/NEJMc1513236
Domínguez-Escobar, J., Chastanet, A., Crevenna, A. H., Fromion, V., Wedlich-Söldner, R., & Carballido-López, R. (2011). Processive movement of MreB-associated cell wall biosynthetic complexes in bacteria. *Science*, *333*(6039), 225–228. http://doi.org/10.1126/science.1203466
Eskandarian, H. A., Odermatt, P. D., Ven, J. X. Y., Hannebelle, M. T. M., Nievergelt, A. P., Dhar, N., et al. (2017). Division site selection linked to inherited cell surface wave troughs in mycobacteria. *Nature Microbiology*, *2*(9), 17094. http://doi.org/10.1038/nmicrobiol.2017.94
Garner, E. C., Bernard, R., Wang, W., Zhuang, X., Rudner, D. Z., & Mitchison, T. (2011). Coupled, Circumferential Motions of the Cell Wall Synthesis Machinery and MreB Filaments in B. subtilis. *Science*, *333*(6039), 222–225. http://doi.org/10.1126/science.1203285
Gibson, D. G., Young, L., Chuang, R.-Y., Venter, J. C., Hutchison, C. A., & Smith, H. O. (2009). Enzymatic assembly of DNA molecules up to several hundred kilobases. *Nature Methods*, *6*(5), 343–345. http://doi.org/10.1038/nmeth.1318
Global Tuberculosis Report 2017. (2017). Global Tuberculosis Report 2017, 1–262.
Gonzalo, X., & Drobniewski, F. (2013). Is there a place for β-lactams in the treatment of multidrug-resistant/extensively drug-resistant tuberculosis? Synergy between meropenem and amoxicillin/clavulanate. *The Journal of Antimicrobial Chemotherapy*, *68*(2), 366–369. http://doi.org/10.1093/jac/dks395
González-Leiza, S. M., de Pedro, M. A., & Ayala, J. A. (2011). AmpH, a bifunctional DD-endopeptidase and DD-carboxypeptidase of Escherichia coli. *Journal of Bacteriology*, *193*(24), 6887–6894. http://doi.org/10.1128/JB.05764-11
Gupta, R., Lavollay, M., Mainardi, J.-L., Arthur, M., Bishai, W. R., & Lamichhane, G. (2010). The Mycobacterium tuberculosis protein LdtMt2 is a nonclassical transpeptidase required for virulence and resistance to amoxicillin. *Nature Medicine*, *16*(4), 466–469. http://doi.org/10.1038/nm.2120
Hett, E. C., & Rubin, E. J. (2008). Bacterial growth and cell division: a mycobacterial perspective. *Microbiology and Molecular Biology Reviews : MMBR*, *72*(1), 126–56–table of contents. http://doi.org/10.1128/MMBR.00028-07
Hugonnet, J.-E., Tremblay, L. W., Boshoff, H. I., Barry, C. E., & Blanchard, J. S. (2009). Meropenem-clavulanate is effective against extensively drug-resistant Mycobacterium tuberculosis. *Science*, *323*(5918), 1215–1218. http://doi.org/10.1126/science.1167498
Hussain, S., Wivagg, C. N., Szwedziak, P., Wong, F., Schaefer, K., Izore, T., et al. (2018). MreB filaments align along greatest principal membrane curvature to orient cell wall synthesis. *eLife*, *7*, e32471. http://doi.org/10.7554/eLife.32471
Kieser, K. J., & Rubin, E. J. (2014). How sisters grow apart: mycobacterial growth and division. *Nature Publishing Group*, *12*(8), 550–562. http://doi.org/10.1038/nrmicro3299
Kieser, K. J., Baranowski, C., Chao, M. C., Long, J. E., Sassetti, C. M., Waldor, M. K., et

al. (2015a). Peptidoglycan synthesis in Mycobacterium tuberculosis is organized into networks with varying drug susceptibility. *Proceedings of the National Academy of Sciences of the United States of America*, *112*(42), 13087–13092. http://doi.org/10.1073/pnas.1514135112

Kieser, K. J., Boutte, C. C., Kester, J. C., Baer, C. E., Barczak, A. K., Meniche, X., et al. (2015b). Phosphorylation of the Peptidoglycan Synthase PonA1 Governs the Rate of Polar Elongation in Mycobacteria. *PLoS Pathogens*, *11*(6), e1005010. http://doi.org/10.1371/journal.ppat.1005010

Koschwanez, J. H., Carlson, R. H., & Meldrum, D. R. (2009). Thin PDMS films using long spin times or tert-butyl alcohol as a solvent. *PLoS ONE*, *4*(2), e4572. http://doi.org/10.1371/journal.pone.0004572

Kumar, P., Arora, K., Lloyd, J. R., Lee, I. Y., Nair, V., Fischer, E., et al. (2012). Meropenem inhibits D,D-carboxypeptidase activity in Mycobacterium tuberculosis. *Molecular Microbiology*, *86*(2), 367–381. http://doi.org/10.1111/j.1365-2958.2012.08199.x

Kuru, E., Hughes, H. V., Brown, P. J., Hall, E., Tekkam, S., Cava, F., et al. (2012). In Situ Probing of Newly Synthesized Peptidoglycan in Live Bacteria with Fluorescent D-Amino Acids. *Angewandte Chemie International Edition*, *51*(50), 12519–12523. http://doi.org/10.1002/anie.201206749

Kuru, E., Lambert, C., Rittichier, J., Till, R., Ducret, A., Derouaux, A., et al. (2017). Fluorescent D-amino-acids reveal bi-cellular cell wall modifications important for Bdellovibrio bacteriovorus predation. *Nature Microbiology*, *2*(12), 1648–1657. http://doi.org/10.1038/s41564-017-0029-y

Kuru, E., Tekkam, S., Hall, E., Brun, Y. V., & Van Nieuwenhze, M. S. (2014). Synthesis of fluorescent D-amino acids and their use for probing peptidoglycan synthesis and bacterial growth in situ. *Nature Protocols*, *10*(1), 33–52. http://doi.org/10.1038/nprot.2014.197

Lavollay, M., Arthur, M., Fourgeaud, M., Dubost, L., Marie, A., Veziris, N., et al. (2008). The Peptidoglycan of Stationary-Phase Mycobacterium tuberculosis Predominantly Contains Cross-Links Generated by L,D-Transpeptidation. *Journal of Bacteriology*, *190*(12), 4360–4366. http://doi.org/10.1128/JB.00239-08

Lebar, M. D., May, J. M., Meeske, A. J., Leiman, S. A., Lupoli, T. J., Tsukamoto, H., et al. (2014). Reconstitution of peptidoglycan cross-linking leads to improved fluorescent probes of cell wall synthesis. *Journal of the American Chemical Society*, *136*(31), 10874–10877. http://doi.org/10.1021/ja505668f

Long, J. E., DeJesus, M., Ward, D., Baker, R. E., Ioerger, T., & Sassetti, C. M. (2015). Identifying Essential Genes in <Emphasis Type="Italic">Mycobacterium tuberculosis</Emphasis> by Global Phenotypic Profiling. In *Gene Essentiality* (Vol. 1279, pp. 79–95). New York, NY: Humana Press, New York, NY. http://doi.org/10.1007/978-1-4939-2398-4_6

Mainardi, J.-L., Hugonnet, J.-E., Rusconi, F., Fourgeaud, M., Dubost, L., Moumi, A. N., et al. (2007). Unexpected inhibition of peptidoglycan LD-transpeptidase from Enterococcus faecium by the beta-lactam imipenem. *Journal of Biological Chemistry*, *282*(42), 30414–30422. http://doi.org/10.1074/jbc.M704286200

Murphy, K. C., Papavinasasundaram, K., & Sassetti, C. M. (2015). Mycobacterial recombineering. *Methods in Molecular Biology (Clifton, N.J.)*, *1285*, 177–199.

961 http://doi.org/10.1007/978-1-4939-2450-9_10
962 Paintdakhi, A., Parry, B., Campos, M., Irnov, I., Elf, J., Surovtsev, I., & Jacobs-Wagner,
963 C. (2016). Oufti: an integrated software package for high-accuracy, high-throughput
964 quantitative microscopy analysis. *Molecular Microbiology*, *99*(4), 767–777.
965 http://doi.org/10.1111/mmi.13264
966 Papp-Wallace, K. M., Endimiani, A., Taracila, M. A., & Bonomo, R. A. (2011).
967 Carbapenems: past, present, and future. *Antimicrobial Agents and Chemotherapy*,
968 *55*(11), 4943–4960. http://doi.org/10.1128/AAC.00296-11
969 Pisabarro, A. G., de Pedro, M. A., & Vázquez, D. (1985). Structural modifications in the
970 peptidoglycan of Escherichia coli associated with changes in the state of growth of
971 the culture. *Journal of Bacteriology*, *161*(1), 238–242.
972 Qiao, Y., Lebar, M. D., Schirner, K., Schaefer, K., Tsukamoto, H., Kahne, D., & Walker,
973 S. (2014). Detection of lipid-linked peptidoglycan precursors by exploiting an
974 unexpected transpeptidase reaction. *Journal of the American Chemical Society*,
975 *136*(42), 14678–14681. http://doi.org/10.1021/ja508147s
976 Qiao, Y., Srisuknimit, V., Rubino, F., Schaefer, K., Ruiz, N., Walker, S., & Kahne, D.
977 (2017). Lipid II overproduction allows direct assay of transpeptidase inhibition by β-
978 lactams. *Nature Chemical Biology*, *13*(7), 793–798.
979 http://doi.org/10.1038/nchembio.2388
980 Rebets, Y., Lupoli, T., Qiao, Y., Schirner, K., Villet, R., Hooper, D., et al. (2014).
981 Moenomycin resistance mutations in Staphylococcus aureus reduce peptidoglycan
982 chain length and cause aberrant cell division. *ACS Chemical Biology*, *9*(2), 459–
983 467. http://doi.org/10.1021/cb4006744
984 Rego, E. H., Audette, R. E., & Rubin, E. J. (2017). Deletion of a mycobacterial divisome
985 factor collapses single-cell phenotypic heterogeneity. *Nature*, *546*(7656), 153–157.
986 http://doi.org/10.1038/nature22361
987 Sanders, A. N., Wright, L. F., & Pavelka, M. S. (2014). Genetic characterization of
988 mycobacterial L,D-transpeptidases. *Microbiology (Reading, England)*, *160*(Pt 8),
989 1795–1806. http://doi.org/10.1099/mic.0.078980-0
990 Schindelin, J., Arganda-Carreras, I., Frise, E., Kaynig, V., Longair, M., Pietzsch, T., et
991 al. (2012). Fiji: an open-source platform for biological-image analysis. *Nature*
992 *Methods*, *9*(7), 676–682. http://doi.org/10.1038/nmeth.2019
993 Synergism Testing: Broth Microdilution Checkerboard and Broth Macrodilution Methods.
994 (2016). Synergism Testing: Broth Microdilution Checkerboard and Broth
995 Macrodilution Methods. In *Clinical Microbiology Procedures Handbook, Fourth*
996 *Edition* (pp. 5.16.1–5.16.23). American Society of Microbiology.
997 http://doi.org/10.1128/9781555818814.ch5.16
998 Thangawng, A. L., Ruoff, R. S., Swartz, M. A., & Glucksberg, M. R. (2007). An ultra-thin
999 PDMS membrane as a bio/micro-nano interface: fabrication and characterization.
1000 *Biomedical Microdevices*, *9*(4), 587–595. http://doi.org/10.1007/s10544-007-9070-6
1001 Ursell, T. S., Nguyen, J., Monds, R. D., Colavin, A., Billings, G., Ouzounov, N., et al.
1002 (2014). Rod-like bacterial shape is maintained by feedback between cell curvature
1003 and cytoskeletal localization. *Proceedings of the National Academy of Sciences of*
1004 *the United States of America*, *111*(11), E1025–34.
1005 http://doi.org/10.1073/pnas.1317174111
1006 Vollmer, W., Blanot, D., & de Pedro, M. A. (2008a). Peptidoglycan structure and

1007 architecture. *FEMS Microbiology Reviews*, *32*(2), 149–167.
1008 http://doi.org/10.1111/j.1574-6976.2007.00094.x
1009 Vollmer, W., Joris, B., Charlier, P., & Foster, S. (2008b). Bacterial peptidoglycan
1010 (murein) hydrolases. *FEMS Microbiology Reviews*, *32*(2), 259–286.
1011 http://doi.org/10.1111/j.1574-6976.2007.00099.x
1012 Welsh, M. A., Taguchi, A., Schaefer, K., Van Tyne, D., Lebreton, F., Gilmore, M. S., et
1013 al. (2017). Identification of a Functionally Unique Family of Penicillin-Binding
1014 Proteins. *Journal of the American Chemical Society*, *139*(49), 17727–17730.
1015 http://doi.org/10.1021/jacs.7b10170
1016 Zimmermann, L., Stephens, A., Nam, S.-Z., Rau, D., Kübler, J., Lozajic, M., et al.
1017 (2017). A Completely Reimplemented MPI Bioinformatics Toolkit with a New
1018 HHpred Server at its Core. *Journal of Molecular Biology*.
1019 http://doi.org/10.1016/j.jmb.2017.12.007
1020